Modeling Long-term Forest Carbon Spatiotemporal Dynamics With Historical Climate and Recent Remote Sensing Data

Jing M. Chen[1,2]

([1]International Institute of Earth System Science Nanjing University, Nanjing, China;
[2]Department of Geography and Program in Planning University of Toronto,
Toronto M5S 3G3, Canada)

Abstract *Forests have long life cycles of up to several hundred years and longer. They also have very different growth rates at different stages of their life cycles. Therefore the carbon cycle in forest ecosystems has long time scales, making it necessary to consider forest age in estimating the spatio-temporal dynamics of carbon sinks in forests. The focus of this article is to review methods for combining recent remote sensing data with historical climate data for estimating the forest carbon source and sink distribution. Satellite remote sensing provides useful data for the land surface in recent decades. The information derived from remote sensing data can be used for short-term forest growth estimation and for mapping forest stand age for long-term simulations. For short-term forest growth estimation, remote sensing can provide forest structural parameters as inputs to process-based models, including big-leaf, two-leaf, and multi-layered models. These models use different strategies to upscale from leaf to canopy, and their reliability and suitability for remote sensing applications will be examined here. For long-term forest carbon cycle estimation, the spatial distribution of the forest growth rate (net primary productivity, NPP) modeled using remote sensing data in recent years is a critical input. This input can be combined with a forest age map to simulate the historical variation of NPP under the influence of climate and atmospheric changes. Another important component of the forest carbon cycle is heterotrophic respiration in the soil, which depends on the sizes of soil carbon pools as well as climate conditions. Methods for estimating the soil carbon spatial distribution and its separation into pools are described. The emphasis is placed on how to derive the soil carbon pools from NPP estimation in current years with consideration of forest carbon dynamics associated with stand age variation and climate and atmospheric changes. The role of disturbance in the forest carbon cycle and the effects of forest regrowth after disturbance are also considered in this review. An example of national forest carbon budget estimation in Canada is given at the end. It illustrates the importance of forest stand age structure in estimating the national forest carbon budgets and the effects of climate and atmospheric changes on the forest carbon cycle.*

Keywords forest carbon cycle, forest age, disturbance, remote sensing, NBP, NPP, NEP

*Correspondence: Prof. Jing M. Chen, Department of Geography and Program in Planning, University of Toronto, 100 St. George Street, Toronto ,Ontario, Canada M5S 3G3, Tel: (905)755-9381, E-mail: chenj@geog.utoronto.ca

1. Introduction

With rapid increases in greenhouse gas (GHG) emissions to the atmosphere from fossil fuel consumption, land use change and other human activities in recent decades, the rate of GHG buildup in the atmosphere has accelerated in the past decades. Terrestrial ecosystems play an important part in the global cycle and have been absorbing about 2-3 PgC y^{-1} from the atmosphere in the last three decades (Houghton, 2007, Sarmiento et al., 2009). This sink has been highly variable in the last 50 years (Canadell et al., 2007) and appears to have been increasing in the last few decades (Le Quéré et al., 2009), although the uncertainties of these sink estimates as the residual of the global carbon budget are still very large. The durability of this sink would dictate the rate of CO_2 increase in the atmosphere in the near future under a given greenhouse gas emission scenario and would cause considerable uncertainties in projecting the future CO_2 atmospheric concentration and climate change (Cox et al., 1998; Friedlingstein et al., 2006). From the scientific viewpoint, it is therefore critically important to understand the carbon cycle in terrestrial ecosystems and to improve our ability to project its future trend (Tans et al., 1990; Pataki et al. 2003).

The heterogeneous nature of terrestrial ecosystems presents a major challenge in our effort to improve regional and global carbon cycle estimation. Using atmospheric CO_2 measurements at coastal and continental sites, monthly and annual terrestrial carbon sinks and sources for large areas of the globe have been inferred through atmospheric inverse modeling (Gurney et al., 2002; Rodenbeck et al., 2003; Deng et al. 2007; Stephens et al., 2007). These "top-down" results still have considerable uncertainties and don't yet show enough spatial details suitable for ground validation and policy formulation, although the spatial resolution will soon be improved using the forthcoming CO_2 column data to be retrieved from satellite measurements (Crisp and Johnson, 2005; Inoue et al., 2006). Reliable carbon fluxes can be measured with the eddy covariance technique, as used in the many national and regional flux networks (Baldocchi et al., 2001). However, these flux measurements only cover a very small fraction of the total land surface area. Spatial information of the land surface retrievable from space-borne instruments can be used effectively for spatially explicit carbon cycle modeling (Running et al., 1989; Potter et al., 1993; Chen et al., 2003b; Goetz et al., 2005; Ju et al., 2006) for the purpose of both improving the accuracy of regional carbon budget estimation and showing spatial details for ecosystem management purposes.

This review article serves the following purposes: (1) to briefly review basic concepts of the forest carbon cycle, (2) to describe methods for retrieving surface parameters using satellite data that are useful for carbon cycle modeling, (3) to examine methodologies for process-based modeling of the forest growth rate using

remote sensing inputs, (4) to introduce a method for modeling long-term carbon cycle dynamics (including soil) by combining short-term remote sensing data with long-term climate data and to suggest ways to use flux measurements recent years for validating historical carbon flux calculations, and (5) to consider the role of disturbance in forest carbon cycling. Examples of forest carbon sink and source distributions in Canada and China will be shown to demonstrate some of the modeling principles.

2. Basic Concepts of the Forest Carbon Cycle

The terrestrial carbon cycle involves carbon uptake from the atmosphere through photosynthesis and carbon release from the soil and vegetation through respiration and disturbance. Photosynthesis is a process that converts atmospheric CO_2 in the gaseous form into carbohydrates in the solid form. Respiration is a process that returns the CO_2 gas to the atmosphere through consuming some of the carbohydrates in plants and through decomposing dead organic matter in the soil. Disturbance to an ecosystem can occur due to fires, insects and timber harvest, causing additional release of carbon to the atmosphere. The gross primary productivity (GPP) quantifies the total photosynthesis rate per unit land surface area per unit time, usually expressed in units of gC $m^{-2}y^{-1}$ or tC $ha^{-1}y^{-1}$, and it may be considered as the start of the terrestrial carbon cycle. The net primary productivity (NPP) is a measure of net carbon absorption by vegetation per unit time and space, in the form of biomass accumulation. It is responsible for both the increment of total biomass (both aboveground and belowground) with time plus accumulation of soil organic matter through the turnover of fine roots and leaves to soil. In process models, NPP is taken as the difference between GPP and autotrophic respiration (R_a), i.e.,

$$NPP = GPP - R_a \qquad (1)$$

Autotrophic respiration is required to maintain plant life. It has two components: maintenance respiration and growth respiration. Maintenance respiration is the energy cost in maintaining living biomass, and the growth respiration is the energy cost in constructing new plant tissues. These energy costs reduce the rate of biomass production from GPP by about half (Ryan et al., 1996), but the reduction rate depends on growth conditions (Ryan et al., 1997).

The net ecosystem productivity (NEP) determines the net exchange of carbon between the land surface (vegetated or non-vegetated) and the atmosphere, excluding the direct carbon release due to disturbance. It is calculated as the difference between NPP and heterotrophic respiration (R_h), i.e.,

$$NEP = NPP - R_h \qquad (2)$$

R_h results from the decomposition of dead organic matter in soils and the litter layer above mineral soils. By this definition, when NEP>0, the land surface is a sink, i.e., it absorbs more carbon than it releases to the atmosphere. In micrometeorological measurements of carbon fluxes, the term net ecosystem exchange (NEE) is often used (Black et al., 1996). NEE and NEP have the same absolute values but opposite signs.

The net biome productivity (NBP) is used to account for carbon losses due to disturbance at the biome level (Walker and Steffen, 1997). It is estimated as:

$$NBP = NEP - D \qquad (3)$$

where D is the direct carbon release at the time of disturbance. It usually has three components:

$$D = D_{fire} + D_{insect} + D_{\log} \qquad (4)$$

where D_{fire}, D_{insect} and D_{log} are the amounts of carbon release due to forest fire, insect-induced mortality, and accelerated turnover and decomposition of dead organic matter after timber removal, respectively.

NPP is an important component of the terrestrial carbon cycle. For forests, it can be related to biomass increment through tree ring analysis (Thomas et al., 2007). When CO_2 fluxes are measured simultaneously above and below the canopy, half-hourly NPP values can also be derived for model validation (Chen et al., 1999). CO_2 flux measurements directly provide NEP data. The flux data can also be used to derive GPP through adding the total ecosystem respiration (R_e) to the NEP measured in daytime (Goulden et al., 1996). The total ecosystem respiration is the sum of autotrophic and heterotrophic respiration.

3. Remotely Sensed Surface Parameters Useful for Forest Carbon Cycle Modeling

As the land surface is generally heterogeneous, airborne and space-borne remote sensing measurements can provide highly desirable information for modeling some of the carbon cycle components discussed above. There are a long list of land surface parameters that are useful for forest carbon cycle modeling (Chen, 2005), including leaf area index, clumping index, disturbance, land cover, biomass, wetland, leaf chlorophyll, leaf nitrogen, etc. Methods for retrieving the first three parameters are briefly reviewed here, and some examples are also given.

3.1. Leaf Area Index

Leaf area index (LAI) is defined as one half the total leaf area (all sided) per unit ground surface area (Chen and Black, 1992). This definition is suitable for both broadleaf and needleleaf forms and is now broadly accepted (Jonckneere et al., 2004). Several algorithms have been developed for global mapping of LAI using

data from various sensors including MODIS (Myneni et al., 2002), POLDER (Lacaze et al., 2003), MERIS (Baret et al., 2006), and VEGETATION and AATSR (Deng et al., 2006). Large discrepancies are found among these global LAI products (Garrigues et al., 2008). In addition to the differences in sensor characteristics, these LAI retrieval algorithms also differ considerably in techniques used to relate reflected radiative signals to LAI and in assumptions made in establishing these relationships. There are also inconsistencies in LAI definition and in techniques for ground-based LAI measurements used in the algorithm development. In producing and validating Canada-wide LAI products, Chen et al. (2002) proposed a set of LAI measurement protocols as well as validation procedures. Through previous studies (Chen, 1996, Chen et al., 1997; Chen et al., 1999; Chen et al., 2002; Fernandes et al., 2003; Abuelgasim et al., 2005), consistent ground-based measurements of LAI were made in many forest and crop canopies over large geographical areas, providing a solid foundation for LAI map validation over Canada. For conifer forests, it is shown that the reduced simple ratio (RSR) (Brown et al., 2000) is most significantly correlated with LAI, where RSR is defined as

$$RSR = \frac{\rho_n}{\rho_r}(1 - \frac{\rho_s - \rho_{\min}}{\rho_{\max} - \rho_{\min}}) \qquad (5)$$

where ρ_n, ρ_r, and ρ_s are the reflectance in NIR, red, and shortwave infrared (SWIR) bands, respectively, and ρ_{min} and ρ_{min} are the minimum and maximum reflectance in the SWIR band, determined from 1% cutoff points in the histogram of a given image. Figures 1a and 1b show the relationships between LAI and SR and between LAI and RSR for major cover types, respectively. Compared with SR, i.e., ρ_n/ρ_r, RSR has a large sensitivity to LAI changes through suppression of the effects of the background greenness and variability. RSR differs less for the various cover types at the same LAI than does SR, giving a clear advantage for applications to mixed pixels, which are the norm in coarse pixels. RSR are also found to be better correlated to LAI of boreal forests than other vegetation indices (Stenberg et al., 2004). In the LAI algorithm of Deng et al. (2006), RSR is only used for forest cover types, but SR is used for other cover types to avoid the error due to the large influence of irrigation on SWIR reflectance.

The algorithm of Deng et al. (2006) is developed for global LAI mapping based on a geometric-optical model (Chen and Leblanc, 1997 and 2001) calibrated against LAI measurements made in Canada and elsewhere. In this algorithm, the dependence of the reflectance on the solar and satellite view angles, i.e. bi-directional reflectance distribution function (BRDF), is considered using a look-up table technique. The LAI retrieval is made in two steps: (1) to invert the remotely sensed canopy gap fraction into the effective LAI (L_e) (Chen, 1996), assuming the spatial distribution of leaves is random, and (2) to convert the effective L_e into LAI

(L) using the following equation:

$$L = L_e / \Omega \qquad (6)$$

where Ω is the clumping index characterizing the deviation of the leaf spatial distribution from the random case (see Section 3.2 below). Either cover-type specific Ω values or a global Ω map can be used for this conversion. An example of a global LAI map in the mid-summer produced using this algorithm is shown in Figure 2. Partial validation of this map has been made using data from Canada (Pisek et al., 2007) and North America (Pisek and Chen, 2007).

3.2. Clumping Index

When the size of leaves is smaller than the canopy height, Ross (1981) demonstrated that the attenuation of radiation in a plant canopy can be well described by the Beer's law when the leaf spatial distribution is random. Nilson (1971) modified the Beer's law with a leaf dispersion parameter to consider the case when this distribution is not random. The leaf distribution can either be more regular than random, or more clumped than random. Natural ecosystems generally have clumped distributions of leaves, such as groupings of leaves in shrubs and tree crowns, and this dispersion parameter is therefore often called the clumping index (Chen, 1996). Chen and Cihlar (1995) developed an optical instrument named TRAC (Tracing Radiation and Architecture of Canopies) to measure this clumping index based on a gap size distribution theory (Miller and Norman, 1971). Measuring this clumping index has therefore become an integral part of LAI measurements, and a large dataset of clumping index for various ecosystems have been accumulated. However, as the three-dimensional canopy structure varies greatly in space, the clumping index also varies greatly, and it is highly desirable to map this index. It was not possible to do this globally until recently the multi-angle POLDER data become available. Chen et al. (2001) first demonstrated that the magnitude of reflectance variation from the hotspot, where the illumination and observation directions coincide, to the darkspot, where the reflectance is minimum in the principle solar plane, is mostly determined by the degree of foliage organization (clumping). Through geometrical optical simulations using the 4-Scale model (Chen and Leblanc, 1997), they demonstrate that clumped canopies cast strong shadows in the forward viewing directions, reducing the darkspot reflectance. The reduction was found from data and simulations to be the largest for conifer, smallest for grassland. They developed an angular index based on the hotspot and darkspot reflectance. These model simulations were later validated using airborne POLDER data (Lacaze et al., 2002) and space-borne POLDER data (Chen et al., 2003a). Through large number of model simulations (Chen et al., 2005; Leblanc et al., 2005), it is shown that the normalized difference between hotspot and darkspot (NDHD) is most linearly related to the clumping index.

NDHD is defined as:

$$NDHD = \frac{\rho_h - \rho_d}{\rho_h + \rho_d} \quad (7)$$

where ρ_h and ρ_d are the hotspot and darkspot reflectance, respectively. These modeled relationships are applied to multiple angle POLDER data for regional and global clumping index mapping (Chen et al., 2005; and Leblanc et al., 2005). For this purpose, POLDER data for the same pixel observed at different angles (up to 14 angles during one single overpass) are fitted with a simple exponential function (Chen and Cihlar, 1997) to find the most reliable hotspot and darkspot values for a given set of observations. Using these methodologies, Chen et al. (2005) for the first time produced a global clumping index map using POLDER I data at 6 km resolution, and this map is updated here using POLDER III data (Figure 3). This map is a multiple angle view of the global land surface, where forests are most clumped (clumping index much smaller than unity) and grassland is least clumped (clumping index close to unity). This multiple angle view can also tell shrubland from grassland, not possible in a single view image. In forested areas, there are large variations in the index due to forest structural differences and topographical effects. In mountainous areas, topographical variations also contribute to the BRDF variation, causing additional unwanted variation in the retrieved clumping index. The first order of this effect has been removed based on the standard deviation of digital elevation model at 1 km resolution within each 6 km × 6 km POLDER pixel (Pisek et al., 2010). This clumping index map has been used to convert effective LAI maps derived using the algorithm of Deng et al. (2006) to true LAI maps (Chen et al., 2010).

3.3. Disturbance Detection

Disturbance to forests occurs mostly due to wildfires, insects and timber harvest. It has profound consequences in forest carbon cycling through its impacts on biomass, soil organic matter, stand dynamics, forest renewals and succession, etc. (Kurz and Apps, 1999). The changes caused by disturbance can be reliably detected using remote sensing techniques. After a forest is burned, for example, green leaf area and the standing liquid water in foliage and stem biomass are drastically reduced, causing the reflectance in near-infrared (NIR) to decrease and the reflectance in mid-infrared (MIR) to increase. The ratio of MIR to NIR reflectance therefore increases dramatically shortly after fire disturbance. Figure 4, shows the variation of this ratio obtained from SPOT VEGETATION images in the summer 1998 with time since fire for all burned fire scars across Canada since 1959 (Amiro et al., 2002). The correlation is improved when separate regressions are made for individual ecoregions in Canada, with r^2=0.57-80 for 16 of the 18 ecoregions (Amiro and Chen, 2002). As the variation in this ratio becomes small in about 25 years after fire, fire scar dating was restricted to 25 years before the

imaging date in 1998, with an error of ±7 years. When images acquired in multiple years are used, the accuracy in fire scar mapping and dating can be further improved (Zhang et al., 2004).

The ratio of MIR and NIR reflectance is used as a general disturbance index (DI) in our recent work (He et al., 2010a) because it also responds to other disturbance types including insect and harvest. For the purpose of refining a forest stand age map over conterminous USA compiled using Forest Inventory and Analysis (FIA) data at the county level, spatial information of forest disturbance and its occurrence date would be useful. For this purpose, over 400 pairs of Landsat TM/ETM scenes acquired circa 1990 and 2000 were used to detect forest disturbance in the period between 1990 and 2000 (He et al., 2010a). The data were preprocessed by the Landsat Ecosystem Disturbance Adaptive Processing System (LEDAPS) project (Masek et al., 2008), and the spatial resolution of the original images was reduced from 30 m to 500 m for computation efficiency. The detected disturbances based on the change in DI between 1990 and 2000 were separated into two five-year age groups according the DI value. FIA data of forested areas in various forest stand age groups at the county level were used to set the thresholds for disturbance detection and for separating the detected disturbance in two groups, i.e. disturbance between 1990 and 1995 and between 1996 and 2000. The results are shown in Figure 5, where the date of detected disturbance is converted to the stand age assuming the regrowth of a forest starts in the second year of the disturbance. The disturbance is mostly caused by fire in western states, by insect in northeastern states, and by harvest in southeastern states.

4. Photosynthesis Modeling Methodology

The total photosynthesis in a vegetation stand, e.g. at the canopy level, is the sum of the contributions from individual leaves. The biochemical processes that take place inside individual leaves during photosynthesis are therefore of fundamental importance in our ability to simulate photosynthesis at the canopy level. When a photosynthesis model for individual leaves is available, various upscaling strategies can be used to estimate the canopy-level photosynthesis. Remotely sensed vegetation structural parameters, i.e. LAI and clumping index, described above are essential for this upscaling.

4.1. **Leaf-level photosynthesis model**

Among models of photosynthetic CO_2 assimilation by plant leaves, the mechanistic model proposed by Farquhar et al. (1980) has been widely used. The model describes the leaf gross photosynthesis rate at an instant of time for C_3 plants as the minimum of:

$$W_c = V_m \frac{C_i - \Gamma}{C_i + K} \quad (8a)$$

and

$$W_j = J \frac{C_i - \Gamma}{4.5C_i + 10.5\Gamma} \quad (8b)$$

where W_c and W_j are Rubisco-limited and light-limited gross photosynthesis rates in μmol m^{-2} s^{-1}, respectively. V_m is the maximum carboxylation rate in μmol m^{-2} s^{-1}; J is the electron transport rate in μmol m^{-2} s^{-1}; C_i is the intercellular CO_2 concentration; Γ is the CO_2 compensation point without dark respiration; K is a function of enzyme kinetics. The dimension for C_i, Γ, K can be either in Pa or in ppm (parts per million). Pa is used here. Both Γ and K are temperature-dependent parameters. Γ, derived from Collatz et al. (1991) and Sellers et al. (1992), can be expressed as:

$$\Gamma = 1.92*10^{-4}\, O_2(1.75)^{(T-25)/10} \quad (9)$$

where O_2 is the oxygen concentration in the atmosphere, being 21,000 Pa, assuming that the atmospheric pressure is 100,000 Pa and O_2 occupies 21% of the air by volume. T is the air temperature in ^oC. K is given by:

$$K=K_c(1+O_2/K_o) \quad (10)$$

where K_c and K_o are Michaelis-Menten constants for CO_2 and O_2 in Pa, respectively. $K_c = 30*2.1^{(T-25)/10}$, and $K_o = 30{,}000*1.2^{(T-25)/10}$ (Collatz et al., 1991). V_m can be expressed as a function of temperature (Collatz et al., 1991) or a function of both temperature and leaf nitrogen content (Bonan, 1995):

$$V_m = V_{m25}\, 2.4^{(T-25)/10} f(T) f(N) \quad (11)$$

where V_{m25} is V_m at 25 ^oC, and is a variable depending on vegetation type, $f(T)$ and $f(N)$ are temperature and nitrogen limitation terms defined as:

$$f(T)=(1+\exp((-220{,}000+710(T+273))/(R_{gas}(T+273)))))^{-1} \quad (12a)$$

$$f(N)=N/N_m, \quad (12b)$$

where N is the leaf nitrogen content, and N_m is the maximum nitrogen content. J is dependent on photosynthetic photon flux density ($PPFD$) absorbed by the leaf (Farquhar and Caemmerer, 1982) and is given by:

$$J=J_{max}PPFD/(PPFD+2.1*J_{max}) \quad (13)$$

where J_{max} is the light-saturated rate of electron transport in the photosynthetic carbon reduction cycle in leaf cells. According to Wullschleger (1993), it is related to the Rubisco activity by:

$$J_{max}=29.1+1.64*V_m. \quad (14)$$

To get net CO_2 assimilation rate (A), daytime leaf dark respiration (R_d) is subtracted from Eq. 8:

$$A=min(W_c, W_j)-R_d. \quad (15)$$

According to Collatz et al. (1991),

$$R_d=0.015V_m. \quad (16)$$

The above instantaneous photosynthesis model at leaf level defines the photosynthetic processes of individual leaves with known light illuminance at an instant of time. In using the above equations to calculate the photosynthesis rate of a leaf, the value of C_i is unknown, and another physically based equation is needed as described below.

The net photosynthesis rate can also be described in the form (Leuning, 1990; Sellers et al., 1996):

$$A = (C_a - C_i)g \quad (17)$$

where C_a is CO_2 concentration in the atmosphere; g is the conductance to CO_2 through the pathway from the atmosphere outside of leaf boundary layer in μmol m^{-2} s^1 Pa^{-1} to the intercellular space, given by:

$$g \approx 10^6 * g_s /(R_{gas} *(T+273)) \quad (18)$$

where g_s is stomatal conductance; R_{gas} is the molar gas constant, being 8.3143 m^3 Pa mol^{-1} K^{-1}. After (i) substituting C_i in Eqs. 8a & 8b with Eq. 14, (ii) combining the results with Eq. 15, and (iii) choosing the solution of the quadratic equations with the smaller roots (Leuning, 1990), we obtain:

$$A_c = \frac{1}{2}((C_a + K)g + V_m - R_d - \sqrt{((C_a + K)g + V_m - R_d)^2 - 4(V_m(C_a - \Gamma) - (C_a + K)R_d)g}\ ) \quad (19a)$$

$$A_j = \frac{1}{2}((C_a + 2.3\Gamma)g + 0.2J - R_d - \sqrt{((C_a + 2.3\Gamma)g + 0.2J - R_d)^2 - 4(0.2J(C_a - \Gamma) - (C_a + 2.3\Gamma)R_d)g}\ ) \quad (19b)$$

where A_c and A_j correspond to W_c and W_j, respectively, after a small reduction for dark respiration.

4.2. Canopy-level photosynthesis models

In principle, Eqs. 19a and 19b could be applied to every leaf in a canopy in order to simulate the canopy-level photosynthesis rate. However, in practice there are several ways to use the individual leaf model for the whole canopy. The principles of these ways of modeling are described here.

4.2.1 Big-leaf model

It is assumed in using a big-leaf model that biochemical processes that are described at the leaf-level are unchanged at the canopy level, i.e. Eqs. 8-19 can all be applied to the canopy treated as one single "big leaf". Under the same meteorological and soil conditions, the big leaf can function differently according to one single parameter: leaf area index (L). It is used to define the canopy conductance (g_c):

$$g_c = L \times g \qquad (20)$$

This canopy conductance is used to replace the stomatal conductance g in Eq. 17 to change the single leaf model to a big-leaf model. To recognize the fact that not all leaves in the canopy contribute equally to the total canopy-level photosynthesis, some big-leaf models (Seller et al., 1992 and 1996) made adjustments to Eq. 20 by weighting the contributions of leaves at different depths into the canopy according to the mean radiation gradient. This adjustment addresses the issue of diminishing contributions of leaves at the lower levels because of the exponential decrease of light with depth into the canopy.

Because of its simplicity and apparent inclusion of biochemical processes, the big-leaf formulation was widely used in early ecological models, such as Biome-BGC (Hunt and Running, 1992, Kimball et al., 1997; Liu et al., 1997) and SiB2 (Sellers et al., 1996). However, big-leaf models have two serious deficiencies (Chen et al., 1999). First, the influence of radiation on photosynthesis is almost non-existent in big-leaf models during the growing season. Even under overcast conditions, sky radiation is still nearly sufficient for the big leaf exposing fully to the incoming radiation, while in reality, shaded leaves or leaves at the lower levels would have insufficient light for photosynthesis. Mathematically, Eq. 8b for the light-limited case produces values consistently larger than those produced by Eq. 8a for the nutrient-limited case, practically diminishing the radiation control over the photosynthesis. In reality, the radiation control operates against shaded leaves in the canopy most of the time. Second, big-leaf models assume that photosynthesis takes place in one leaf (or conceptually one layer of leaves), while in reality several layers of leaves operate simultaneously. This assumption dramatically distorts the carbon flow path, represented as a network of resistances (Figure 6). In the big-leaf formulation, only one leaf internal resistance operates against the flow of CO_2 from the stomatal cavity (represented by C_i) to the photosynthetic apparatus (represented by the compensation point Γ). The use of canopy resistance rather than the stomatal resistance modifies part of the pathway to consider the fact that the carbon flow would meet less resistance through multiple stomatal openings. This description of the flow pathway is quite different from the case of multiple layers of leaves that are operating simultaneously, where several internal leaf resistances operates in parallel, as they occur in reality. The big-leaf formulation therefore artificially amplifies the control of leaf internal resistance on photosynthesis, making it less variable under various environmental conditions as demonstrated by Chen et al. (1999) using daily NPP data derived from two level CO_2 flux measurements. It has been proposed that big-leaf formulation should be abandoned completely (Chen et al., 2003a).

4.2.2. Two-leaf model

To avoid the deficiencies of the big-leaf model formulation as described above, the total canopy photosynthesis (A_{canopy}) can be modeled based on two representative leaves, one sunlit and one shaded (Leuning et al.,1995; De Pury and Farquhar, 1997; Wang and Leuning, 1998). The photosynthesis rates of these two leaves can be calculated using the individual leaf model (Eqs. 8-19) and then multiplied by their respective leaf area indices as proposed by Norman (1982):

$$A_{canopy} = A_{sun} L_{sun} - A_{shade} L_{shade} \quad (21)$$

where the subscripts "sun" and "shade" denote the sunlit and shaded components of photosynthesis and LAI. It is important to note that this two-leaf formulation is conceptually very different from two big-leaf models, in which the total photosynthesis rates for sunlit and shaded leaf strata are calculated using separate sunlit and shaded canopy conductances. Two big-leaf models is an improvement over big-leaf models, but still suffer the same deficiencies as big-leaf models as outlined in Section 3.2.1, although to a lesser extent. We therefore need to differentiate the concepts of "two-leaf model" and "two big-leaf model".

The method of Norman (1982) for calculating LAI_{sun} and LAI_{shade} has been modified to consider the effect of foliage clumping index (Ω) on the canopy radiation regime (Chen et al., 1999):

$$L_{sun} = 2\cos\theta(1-\exp(-0.5\Omega L/\cos\theta)) \quad (22a)$$

$$L_{shade} = L - L_{sun} \quad (22b)$$

where L is the leaf area index, and θ is the solar zenith angle. Ω is 0.5-0.7 for conifer forests, 0.7-0.9 for broadleaf forests, and 0.9-1.0 for grass and crops (Chen, 1996a; Chen et al., 1997). The larger Ω departs from unity, the more non-random is the foliage spatial distribution. It is critically important to consider this factor in productivity models because foliage clumping alters the way plants interact with incident radiation. Increasing foliage clumping (decreasing Ω value) allows more radiation to penetrate through the canopy without being intercepted by the foliage and therefore decreases sunlit LAI and increases shaded LAI. The clumped architecture of forest canopies makes the stratification between sunlit and shaded leaves essential because the fraction of the shaded leaves is much larger in clumped canopies than in random canopies and shaded leaves play an important role in forest productivity (Guolden et al., 1997). In a global GPP modeling study using a two-leaf model, Chen et al. (2010) found that shaded leaves contribute 61%, 48%, 44%, 29%, 39%, and 42% to the total GPP for broadleaf evergreen forest, broadleaf

deciduous forest, conifer forest, shrub, C4 vegetation, and other vegetation, respectively. This result indicates the importance of modeling shaded leaf photosynthesis.

In the calculation of A_{sun} and A_{shade} in Eq. 21, the solar irradiances on the representative sunlit and shaded leaves must be estimated. For remote sensing applications, Chen et al. (1999) developed a set of simple equations for estimating these irradiances from the global radiation according to LAI, clumping index, solar zenith angle and mean leaf inclination angle. These equations also include radiation multiple scattering inside the canopy.

4.2.3. Multi-layer model

The total canopy photosynthesis rate can also be estimated using multi-layer models, in which the average photosynthesis rate of a leaf layer can be estimated using the leaf level model (Eqs. 8-19) in the following mathematical formulation (Bonan, 1995; Foley et al., 1996):

$$A_{canopy} = \sum_{i=1}^{L} A_i(g_i) \qquad (23)$$

where $A_i(g_i)$ is the photosynthesis rate for i^{th} layer of leaves as a function of the average stomatal conductance g_i for that layer. This formulation also avoids the deficiencies of big-leaf models (section 3.2.1), and it has the advantage of specifying different leaf biophysical parameters for different layers, such as the specific leaf area (Raulier et al., 1999) and the leaf nitrogen content (Leuning et al., 1995). In the implementation of this model, it is critical to calculate the average solar irradiance on each layer of leaves in order to obtain the representative value g_i. However, in each layer at a given time, there are sunlit and shaded leaves operating at very different rates, and which of the two limitations (light or Rubisco) takes control depends mostly on whether a leaf is sunlit or shaded. This multilayer formulation is therefore generally not as effective as the simpler two-leaf model. However, it can be further improved by separating the sunlit and shaded leaf groups in each layer (Leuning et al., 1995; Raulier et al., 1999).

4.3 Stomatal conductance

Plants respond to their environment through stomatal movement that can be quantified in terms of stomatal conductance. In all leaf-level and canopy-level photosynthesis models, leaf stomatal conductance to CO_2 is a critical parameter. Two approaches are commonly used in estimating the stomatal conductance and are outlined here.

4.3.1 Jarvis' Semi-empirical Approach

The Jarvis' approach is to reduce a species-dependent maximum stomatal conductance by the degrees of environmental conditions departing from the optimum (Jarvis and Morison, 1981; Running and Coughlan, 1988; Chen et al., 2005). The environmental factors usually include photosynthetic photon flux density (PPFD), temperature (T), vapor pressure deficit (VPD), and soil water content (θ), i.e.

$$g_s = max(g_{max} * f(PPFD) * f(T) * f(VPD) * f(\vartheta_{sw}), g_{min}) \quad (24)$$

where the environmental functions are scalars between 0 and 1, which are formed in the same way as in BIOME-BGC. These functions are expressed as:

$$f(PPFD) = PPFD * PPFD_{coef} / (1 + PPFD * PPFD_{coef}) \quad (25a)$$

$$f(T) = \begin{cases} \ln(T) / \ln(T_{opt}) & T < T_{opt} \\ \cos(\frac{\pi}{2}(T - T_{opt}) / (T_{range} - T_{opt})) & T > T_{opt} \\ 0 & T < 1 \end{cases} \quad (25b)$$

$$f(VPD) = \begin{cases} 1 & VPD < VPD_{open} \\ (VPD_{close} - VPD) / (VPD_{close} - VPD_{open}) & VPD_{open} < VPD < VPD_{close} \\ 0 & VPD > VPD_{close} \end{cases} \quad (25c)$$

$$f(\theta_{sw}) = \begin{cases} 0 & \theta_{sw} \le \theta_{wp} \\ \dfrac{\theta_{sw} - \theta_{wp}}{\theta_{fc} - \theta_{wp}} & \theta_{wp} < \theta_{sw} \le \theta_{fc} \\ 1 - 0.5 \times \dfrac{\theta_{sw} - \theta_{fc}}{\theta_s - \theta_{fc}} & \theta_{fc} < \theta_{sw} \le \theta_s \end{cases} \quad (25d)$$

The meaning of the symbols in these equations and their values and units are found in Table 1.

4.3.2. Ball-Berry's Approach

The recognition of the influence of leaf photosynthesis on leaf stomatal opening has lead to an alternative approach for calculating stomatal conductance. Wong et al. (1979) first reported this influence and argued that plants would regulate stomatal opening to keep the intercellular CO_2 concentration nearly constant (at about 70% of the free air value for C_3 plants). Ball (1988), Leuning (1990), and Collatz et al. (1991) conducted further

laboratory experiments and developed a model that mechanistically links stomatal conductance to leaf net photosynthesis (A_n) in the following manner:

$$g_s = m\frac{A_n h_s}{C_s}p + b, \qquad (26)$$

where g_s is expressed in mol m^{-2} s^{-1}, m is a plant species dependent coefficient, h_s is the relative humidity at the leaf surface, p is the atmospheric pressure, C_s is the CO_2 concentration at the leaf surface, and b is a small value due to leaf dark respiration. This formulation is often called the "Ball-Berry" model to recognize the first two contributors to this theory. Collatz et al. (1991) tested the model and showed good agreement between predicted and measured g_s values over a wide range of leaf temperatures.

The Ball-Berry model revolutionized our understanding of plant physiology: plants keep stomates open for the need of getting CO_2 for photosynthesis while water loss through stomates is a passive consequence. This understanding has a profound implication in modeling the land surface energy budget: for the estimation of evapotranspiration using the Penman-Monteith equation, the stomatal conductance to water would depend on leaf photosynthesis. Advanced land surface schemes have therefore incorporated photosynthesis routines for the purpose of estimating stomatal conductance for water (Sellers et al., 1996; Dickinson et al., 1998; Cox et al., 1998; Dai et al., 2003). However, it is not straightforward to use the Ball-Barry model for stomatal conductance estimation because A_n cannot be estimated without knowing g_s, and an iteration procedure has to be used to determine A_n and g_s simultaneously. This iteration is computationally expensive, and therefore the Ball-Barry model has not been used in many ecological models, especially those developed for remote sensing applications, such as Biome-BGC (Kimbal et al., 1997) and BEPS (Liu et al., 2002). Baldocchi et al. (1994) proposed an analytical solution to g_s estimation without computing A_n explicitly. This would help improve the computation speed for instantaneous leaf photosynthesis, but the methodology needs to be further developed for daily or longer time step calculations.

It should be noted that the Ball-Barry model contains empirical coefficients m and b, and they can vary greatly among different plant species or functional types (Medlyn et al., 1999a and 1999b. The model also does not take into account the effect of soil water stress on stomatal conductance and needs to be further parameterized. This effect may be considered by decreasing either the stomatal conductance directly using a soil moisture scalar (Foley, 1994; Wang and Leuning, 1998; Knorr, 2000) or the photosynthetic rate (Cox et al., 1998) in response to soil water stress.

5. Respiration Modeling Methodology

5.1 Autotrophic respiration

Autotrophic respiration releases CO_2 back to the atmosphere by consuming carbohydrates formed through photosynthesis. Conventionally, autotrophic respiration (R_a) is separated into maintenance respiration (R_m) and growth respiration (R_g) (Amthor, 1989; Running and Coughlan, 1988; Ryan, 1991):

$$R_a = R_m + R_g = \sum_i (R_{m,i} + R_{g,i}) \quad (27)$$

where i is an index for different plant components, (1 for leaf, 2 for stem, and 3 for root).

Maintenance respiration is temperature-dependent:

$$R_{m,i} = M_i \, r_{m,i} \, Q_{10}^{(T - T_b)/10} \quad (28)$$

where M_i is biomass (sapwood for stems) of plant component i; $r_{m,i}$ is maintenance respiration coefficient for component i to estimate the respiration rate at the base temperature at 10ºC; Q_{10} is the temperature sensitivity factor, and T_b is the base temperature. The stem biomass is difficult to obtain for large areas, but the sapwood biomass can be related to LAI retrievable from optical remote sensing. Autotrophic respiration is more closely related to sapwood biomass than the total stem biomass (Lavigne and Ryan, 1997). Growth respiration is generally considered to be not directly dependent of temperature and is proportional to GPP:

$$R_{g,i} = r_{g,i} r_{a,i} (GPP - R_m) \quad (29)$$

where $r_{g,i}$ is a growth respiration coefficient for plant component i; and $r_{a,i}$ is the carbon allocation fraction for plant component i. The recommended values of these respiration coefficients are given in Table 1.

5.2 Heterotrophic Respiration

Heterotrophic respiration results from microbes decomposing dead organic matter in the soil, causing release of CO_2 to the atmosphere. It involves complex physical, biological and chemical processes belowground, and mostly depends on the quantity of soil organic matter as well as temperature and soil moisture. While its theoretical temperature dependency (Lloyds and Taylor, 1994) and empirical moisture response curves (Parton et al., 1993) are available, the most difficult task in its regional estimation is to know the spatial distribution of soil organic matter. The decomposability of soil organic matter from different biomass sources (leaves, roots and stems at different times) is quite different under the same environmental conditions, and it is often necessary to separate the total soil carbon into several pools, such as the litter, fine detritus, coarse detritus, fast, slow, and passive pools. The separation and interaction of these pools add to the complexity of heterotrophic respiration estimation.

Measurements for the spatial distribution of the total soil carbon and its separation into the various pools are not possible for a region. This distribution has to be estimated under certain assumptions. Since soil carbon originates from biomass turnover to the soil, the total amount of soil carbon at a given location is proportional to the long-term average NPP at the same location. Naturally, when the total soil carbon becomes stable with time, the long-term averaged heterotrophic respiration would equal NPP, i.e. the carbon gain through the net photosynthesis is balanced by the carbon loss through heterotrophic respiration, making the surface carbon neutral. This is often called the dynamic equilibrium of the carbon cycle.

Under this equilibrium assumption, the heterotrophic respiration is simply made to equal the long-term mean NPP. This is an approach widely used in many models (VEMAP, 1995). If the total respiration coefficient, i.e. the rate of respiration per unit soil carbon, is known, the total carbon pool size can be estimated. Similarly, if the respiration coefficients of the various pools are known, the sizes of the various pools can also be derived under the equilibrium assumption. As there are transfers of carbon among the various pools, a set of differential equations need to be solved for this purpose (Chen et al., 2003b). The equations contain temperature and moisture dependent respiration coefficients for the different pools, corresponding to the general truth that for the same NPP, the substrates in colder regions will contain more carbon than warmer regions. Mathematically, the respiration coefficient for the ith pool (K_i) is calculated as

$$K_i = K_{i\_\max} f_T(T_s) f_P(\frac{P+W}{ET})[f_L(L_s).f_S(T_{sc})] \quad (30)$$

where $K_{i\_\max}$ is the maximum respiration rate coefficient for the ith pool; T_s , P, W and ET are the annual mean soil temperature, precipitation, stored soil water and evapotranspiration, respectively; L_s is the structural lignin content of surface litter and in soils; and T_{sc} represents the silt and clay fractions of mineral soil. f_T , f_P, f_L and f_S are functions of the designated variable in the brackets. In modeling Canada's forest carbon sink and source distribution (Chen et al., 2003b), L_s is estimated from biomass components using methods and coefficients suggested in the literature (Peng et al., 1998; Gholz et al., 2000; Trofymow et al., 1998), and T_{sc} is obtained from the GIS database of Soil Landscapes of Canada (Shields et al., 1991; Schut et al., 1994, see also http://sis.agr.gc.ca/cansis/references/1994ss_a.html). The function $f(\frac{P+W}{ET})$ is an adjustment of heterotrophic respiration for changes in soil water regime (Parton et al., 1993) to evaluate the influence of soil moisture, lignin content and soil texture on organic carbon decomposition rates of the various pools. This adjustment is important for low-lying areas where P is consistently much larger than ET. Under the assumption that decomposition reaches a maximum at 35ºC, the temperature response function is

$$f(T_s) = e^{308.56(\frac{1}{35+46.02} - \frac{1}{T_s+46.02})} \quad (31)$$

This equation is reliable for the mean annual temperature T_s < 35ºC, and for tropical regions, it may be modified.

6. Stand Age as an Important Driver of the Forest Carbon Cycle

The forest carbon cycle is closely associated with the forest life cycle, which can last for several hundred years. A forest life cycle starts with an initial slow growth after regeneration following disturbance or plantation and reaches the maximum growth rate at mid ages. This is generally followed by a gentle decline in growth at old ages. The age, at which a forest stand reaches the maximum growth rate, depends on climate and site conditions. In warmer climates and at better site conditions, the maximum rate is reached earlier. While the growth, i.e. NPP, has large temporal variations associated with stand age at a given location, the soil carbon stock accumulated over long periods of time changes relatively little with age, and the heterotrophic respiration would also change much less than NPP. As a result, measured NEP at different forest stand ages shows variation patterns similar to those of NPP (Law et al., 2003; Coursolle et al., 2006).

In simulating the carbon cycle associated with the forest life cycle, the key is to know how NPP varies with age. Soil carbon pools obtained from spin-up procedures under the equilibrium assumption (Section 4.2) would also vary with NPP as over 50% of NPP is turned to dead organic matter in soil each year. There have been many empirical studies of the variation of aboveground biomass with age for forestry purposes, but empirical relationships between NPP (both aboveground and belowground) and age are very few. Forest inventory data generally include aboveground biomass and mortality at various stand ages. For the purpose of forest carbon cycle modeling concerning not only the accumulation of carbon in biomass but also in soils, these inventory data need to be converted into the net primary productivity (NPP). There are four terms in NPP: (1) life biomass accumulation, (2) mortality of both aboveground and belowground biomass; (3) foliage turnover to soil, and (4) fine root turnover in soil. The last two terms made up for more than 50% of the total NPP. While forest inventories often provide reliable estimates of terms (1) and (2), terms (3) and (4) are most error prone when limited empirical relationships between aboveground biomass and foliage or fine root are used to estimate them. These estimates are most seriously confounded by unknown variations of the turnover rates with stand age as such field information is rare.

In Canada's forest carbon cycle modeling (Chen et al., 2003b), NPP-age relationships (Figure 7) were established from analysis of stand yield data for black spruce in Ontario (Chen et al., 2002). Foliage and fine

root turnover rates were estimated using empirical relationships between total biomass and foliage or fine root biomass. The largest uncertainty in the NPP-age relationships derived this way exists at old ages. The derived NPP-age relationships for boreal forests vary with site conditions quantified using a site index in terms of the tree height that can be reached after 50 years of growth. These relationships show a general temporal pattern of rapid increase in NPP in early ages, peak growth in mid-ages, and slow decline in old ages. For application of these relationships to large areas, a general semi-empirical mathematical function was developed:

$$NPP(age) = A(1 + \frac{b(\frac{age}{c})^d - 1}{\exp(\frac{age}{c})}) \quad (32)$$

where coefficient A, b, c and d are dependent on the site index. The site index was replaced by the mean annual air temperature for Canada-wide NBP modeling (Chen et al., 2003b)

In our recent study (He et al., 2010b), the Forest Inventory and Analysis (FIA) data as compiled by Smith et al. (2002) are used to derive NPP-age relationships for forests in USA. In order to address the issue of the uncertain foliage and fine root turnover rates at different stand ages, we use a leaf area index map in 2000 over USA at 1 km resolution in combination with a forest age map to derive LAI-age relationships. These relationships are then used to establish the corresponding foliage turnover-age relationships using species-specific values for leaf longevity and leaf mass-to-area ratio. These relationships are also used for estimating the fine root turnover rates based on a large sample of measured ratios of fine root to leaf turnover rates. In this way, NPP-age relationships are established for 18 major forest species groups in 10 ecoregions in conterminous USA (Figure 8). The temporal variation patterns shown in Figure 8 are similar to those of boreal forests (Figure 7). However, the patterns are more variable and less clearly defined. In particular, the decline rate at old ages is quite different among the 18 species groups. Some of the curves might have been considerably influenced by forest management practices.

In Figure 7, the absolute NPP values are determined by the site index, while in Figure 8, they represent the mean NPP for the species groups distributed over large geographical areas. For spatially explicit carbon cycle modeling, the absolute NPP value in a given year can be estimated pixel by pixel using remote sensing and other inputs (Section 4), and the historical NPP variation in each pixel (x,y) can be obtained using the following equation:

$$NPP(x, y, t) = NPP(x, y, t_{ref}) \frac{F_{NPP}(x, y, age(t))}{F_{NPP}(x, y, age(t_{ref}))} \quad (33)$$

where t is the time (year) either before or after the reference time (t_{ref}), and $F_{NNP}(x,y,age(t))$ is the normalized NPP-age curve for the pixel (x,y), with values vary between 0 and 1. It is defined as:

$$F_{NPP}(x, y, age(t)) = NPP(x, y, age(t)) / NPP_{Max} \quad (34)$$

where NPP_{Max} is the maximum value in a NPP curve as shown in Figures 7 and 8. The age of the forest in a pixel at a given time t is determined by the forest age in the reference year, $age(t_{ref})$ and the difference between t and t_{ref}, assuming that the increment of forest stand age is one year for each year. The reference year is the year at which an NPP map is available for spatially explicit modeling, and the map can be obtained through process-based modeling at hourly or daily time steps using remote sensing inputs (Section 4). In this way, the absolute NPP values most accurately determined in a reference year is combined with a normalized NPP-age curve to construct the historical variation of the absolute NPP value due to changes in forest stand age. The normalized curve shape not only depends on forest species types but also varies with site conditions.

7. Time Scale of the Carbon Cycle and Its Implications on Carbon Modeling

Different ecosystems have different carbon residence times, with northern ecosystems having much longer carbon residence times than those of tropical and temperate ecosystems (Thompson et al., 1996). The residence time (τ) is taking as the ratio of the total carbon (C) in the ecosystem, including soil and biomass, to the new carbon flux into the system, i.e.

$$\tau = \frac{C}{NPP} \quad (35)$$

For a typical boreal forest with 30 tC/ha in biomass (Chen et al., 2003b), 120 tC/ha in soil (Tarnocai, 1996), and 3 tC/(ha y) of NPP (Liu et al., 2002), the residence time would be 50 years. While for a typical tropical forest with 100 tC/ha in biomass (Neeff et al., 2005), 50 tC/ha in soil (Batjes and Dijkshoon, 1999), and 10 tC/(ha y) of NPP (Krinner et al., 2005), the residence time would be 15 years. As latitude increases, temperature decreases and the carbon residence time in ecosystems increases.

These long carbon residence times, as compared with short water residence times (several weeks), have profound implications on carbon cycle modeling: (i) any model that simulates the net ecosystem productivity for periods shorter than one residence time is incomplete at the best, and in this case the total soil carbon or its decomposition coefficient is often arbitrarily assigned; (ii) any model that does not separate the total carbon into several pools of different residence times would also be in error as the fractions of the different pools would change with time, especially after disturbance; and (iii) as old soil carbon (in the slow and passive pools)

that is accumulated over a long period of time (thousands of years) is still slowly decomposing, a spin-up procedure is needed to estimate the amount of old carbon. This spin-up procedure is often dubbed "model warm-up", and is done either through running the model for a given pixel for 5-20 thousand years (which is time consuming in computation) (Liu et al., 2005) or by solving a set of differential equations under a dynamic equilibrium assumption for the pre-industrial period (Chen et al., 2003b).

8. Strategies to Reduce Uncertainties in Carbon Cycle Estimation

As the carbon balance (NEP) of a forest stand is the small difference between NPP and R_h (Eq. 2) and the errors in both NPP and R_h are considerable, the NEP estimate can be erroneous without using error constraining strategies. For example, for spatially explicit modeling (Liu et al., 2002), the error in NPP is estimated to be about 25%. The error in R_h can be even larger due to the difficulty in determining soil carbon pools and their respiration coefficients under various conditions. The global terrestrial carbon sink in recent decades is about 2 GtC/y (Houghton, 2007), while the global NPP is about 60 GtC/y (VERMAP, 1995), and therefore the sink is only about 3% of NPP when averaged over the global land surface. To model such a small difference based on NPP and R_h with much larger errors, some strategies for reducing the uncertainty in NEP estimation should be followed. They are briefly described as fellows.

1. To estimate the soil carbon pools based on the assumption of a dynamic equilibrium between NPP and R_h in the pre-industrial period (before 1900) (VEMAP, 1995; Chen et al., 2000). Under this assumption, R_h is forced to equal NPP in the preindustrial period so that the effect of any systematic error in NPP on NEP is greatly reduced (Chen et al., 2000), and the error in R_h is forced to cancel that in NPP for the NEP estimation. After the preindustrial period, NEP is allowed to vary according to climate and atmospheric conditions. In this way, the carbon balance estimated for recent years results from the accumulated effects of all changes since the pre-industrial period, and any small effects of climate and atmospheric changes on NEP can be simulated with reasonable accuracy. In spatially explicit modeling, such an equilibrium assumption is made for each pixel, and an error often occurs because of the variable disturbance history at different locations. However, this error would reduce by a factor of $e^{t/\lambda}$, where t is time since the equilibrium assumption and λ is the carbon residence time. If the equilibrium assumption is made twice the residence time prior to the present date, i.e. t/λ=2, the error in disequilibrium at the preindustrial period would reduce by a factor of e^2=7.4. Such an error estimate shows the importance of performing long-term historical simulations of the forest carbon cycle.

An important step in implementing this strategy is to estimate NPP at the preindustrial period, as we often have only estimates of current NPP. Recognizing the issue that NPP may have changed following the historical climate and atmospheric changes, the past variation in NPP since the preindustrial period has to be simulated. An iteration procedure is often used until the historical simulation of NPP agrees with currently available NPP estimates (see more explanation in Section 10). As the historical change in NPP is one of the main reasons for current terrestrial sinks, this implementation of the error reduction strategy is still sensitive to model parameterizations for the effects of climate and atmospheric composition on plant growth.

2. For forest ecosystems, the historical NPP variation is not only caused by climate and atmospheric variations, but also by stand age. An additional strategy is needed to avoid the age effect on the preindustrial equilibrium assumption. This strategy involves the use of the concept of equilibrium stand age, which is the age at which a forest stand becomes carbon neutral as it gets older. During one forest life cycle, there are two times at which the forest carbon cycle is balanced (neutral), one at the early stage when the NPP increases to an extent that offsets the heterotrophic respiration, and the other is at the late stage when the NPP declines to a level that equals heterotrophic respiration. The older age is taken as the equilibrium age because the NPP at this age better represents the long-term mean value for a stand. For managed stands which don't have significant NPP decrease at older ages, the age at which the NPP equals the mean NPP over the mean harvest-regrowth rotation may be taken as the equilibrium age. As the rate of forest growth depends on climate and site conditions, the equilibrium age would vary spatially. In Canada's forest carbon cycle modeling, the equilibrium age is determined on the pixel bases through simulating historical NPP and R_h and find the second age when these two are equal (or within 1% to each other). It is found that this age is between 80 and 150 years for Canada's forests, increasing from south to north.

The equilibrium age concept serves the purpose of a baseline estimate for an "ageless forest" at a given location (pixel). This baseline is used to separate disturbance and non-disturbance effects. With the important preindustrial equilibrium assumption, this ageless baseline provides the best objective estimates of the soil carbon as we generally don't have data for forest age in the preindustrial period.

9. The Influence of Disturbance on the Carbon Cycle

Given the large variation of forest NPP with stand age (Section 6), forest disturbance (fire, harvest, insect) plays particularly important roles in forest carbon cycling because it not only causes direct emission of carbon to the atmosphere but also resets "the forest biological clock" by changing its age structure. The amount of

direct carbon release to the atmosphere during disturbance depends on the type and the severity of disturbance. Fire disturbance typically releases a large amount of carbon in a short duration during disturbance and also a small amount of carbon in subsequent years due to decomposition of dead trees (Stocks, 1991; Amiro et al., 2001), while insect disturbance causes loss of foliage or death of whole trees which gradually decompose over a long period of time. Harvest often leaves debris on site which also gradually decomposes. An accurate forest carbon cycle model should consider (i) the indirect effect of disturbance on the forest carbon cycle through the change in forest age structure; (ii) the direct carbon release during disturbance; and (iii) the indirect carbon release after disturbance due to the decomposition of the affected biomass. In Canada's forest carbon cycle modeling (Chen et al., 2003b), a forest age map at 1 km resolution was used to determine the time of disturbance. Since there is no sufficient information to differentiate disturbance types (fire, insect and harvest) at the pixel level, all disturbances were treated as fire disturbance. The C emissions were estimated as:

$$D_{fire} = B_f + 0.25B_w + L_{detf} \qquad (36)$$

where B_f and B_w are biomass densities of foliage and woody components, respectively; and L_{detf} is the detritus from foliage. As these biomass components are modeled pixel by pixel, it is possible to estimate the carbon release due to disturbance for each disturbed pixel. However, the effect of severity of disturbance (Kasischke et al., 2000) has not been considered. This coefficient of 0.25 for the consumption of woody material is found through adjustment so that the mean emission per unit ground area agrees with estimates of Amiro et al. (2001) and Stocks (1991).

10. Integration of Short-term Remote Sensing Data with Historical Climate Data for Long-term Forest Carbon Cycle Modeling

Satellite remote sensing data allow us to estimate the spatial distribution of NPP in recent years through the use of retrieved surface parameters including land cover, LAI and clumping index. Satellite data are also useful for detecting disturbance that affects forest stand age. These short-term spatially explicit data can be combined with historical climate data for the needed long-term carbon cycle modeling.

A forest age map allows us to determine not only the time of last disturbance for direct carbon release estimation but also forest regrowth after disturbance based on a pre-established NPP-age relationship (Section 6). Figure 9 demonstrates how the forest age information is used for estimating both disturbance and non-disturbance effects on NPP and NEP for a conifer forest

site at mid-latitude in North America. The real climate data and site-level measurements are used in this example. Since this is for the purpose of demonstrating a concept, the actual site information is not provided here. Figure 9a shows the normalized NPP-age curve for this species (based a curve shown in Figure 8). In 2006, this forest was 56 years old, and therefore this site was disturbed in 1950 at which NPP dropped to zero (Figure 9b). Prior to 1950, the forest was assumed to be at a constant equilibrium age because the age at which the forest was last disturbed is unknown. The "climate+CO_2+N" case in Figure 9b represents the variation of the NPP with climate and atmospheric conditions when the forest is assumed to be ageless, where CO_2 and N denotes for the effects of atmospheric CO_2 and nitrogen deposition on NPP. This variation caused by climate and atmosphere is superimposed on the NPP at the equilibrium age, representing the long-term mean NPP of the site. Starting from 1950, forest regrowth begins from zero and increases with time according to the normalized NPP age curve (Figure 9a) and an actual NPP in the reference year 2006, using Eqs. 33 and 34. Because of the historical variation in NPP, the net ecosystem productivity also has a similar historical variation pattern (Figure 9c). Before 1950, the NEP value varies about the neutralilty, but is slightly positive because of the overall positive climate and atmospheric effects. The forest is a large source of carbon shortly after the disturbance in 1950, and as the forest grows after disturbance, it becomes carbon neutral in about 20 years and a carbon sink following the neutrality. The "age only" case represents the effect of forest age variation with time. Before 1950, it is at the equilibrium age and therefore shown as a zero flat line. Climate and other effects are superimposed on this baseline. The measured annual NEP values from 1999 to 1994 using the eddy covariance method are shown as a comparison to the modeled historical NEP values. This comparison suggests that the measured large sinks (large positive NEP) are mostly due to the fact that the forest is at its peak productive age. It would be very erroneous to interpret these large sinks as climate and atmospheric effects by ignoring the forest growth cycle.

This example of NPP and NEP calculations shown in Figure 9 also demonstrates how the NPP value modeled using remote sensing inputs for a recent reference year or a short-term can be used to constrain the long-term forest carbon cycle modeling. In this example, the NPP in the reference year (2006) is used to calculate the historical NPP variation retrospectively according to climate, atmospheric CO_2 and nitrogen deposition as well as forest age at the reference year and a

NPP-age relationship. An iteration procedure is followed to ensure the forward NPP calculation at the reference year agrees with the predetermined NPP at the same year. The NPP value at the beginning of the modeling period (1900 in this case) determined through this iteration is then used to estimate the soil carbon pools based on the dynamic equilibrium assumption. If the stand age is larger than the modeling period (106 years in this case), the equilibrium age is not found within the modeling period, so that the modeling period is moved forward assuming the climate remains the same before 1900. This combination of the short-term remote sensing-based NPP modeling (reference year) and the long-term climate-based modeling can effectively integrate the long-term effects of climate and atmospheric changes as well as disturbance and regrowth. However, the underlying assumption of such long-term modeling is that forest cover types have not changed over the modeling period. More advanced methods need to be developed to consider the impact of forest successional processes and land use changes.

11. Examples from Canada

Extensive research was previously done to estimate Canada's forest carbon budgets based on forest area and age structure data in forest inventories (Kurz and Apps, 1999). In this previous study, biomass-age relationships were derived from the inventories compiled over about 100 years regardless of possible changes in growth conditions over the long period, and these relationships were applied to 48 spatial units over Canada's landmass. The use of remote sensing not only greatly improves the spatial resolution (~1 km) but also allows estimation of changes in forest growth conditions when the past climate and current vegetation data are used in process-based modeling (Chen et al., 2003b). Figure 10 shows the major remote sensing parameters used in Canada-wide forest carbon cycle modeling as well as the major steps. One unique aspect of this modeling approach based on remote sensing is that not only non-disturbance factors (nitrogen and CO_2 fertilization effects, climate variables) are considered, as many process models do, but also disturbance factors (fire, insect, harvest) are explicitly considered, although insect and harvest disturbances are treated as fire disturbance due to lack of spatial data. Of particular importance in modeling the disturbance effects is the forest age map in 1998 (Figure 11) created through combining forest inventory, large fire polygons, and remote sensing data for dating fire scars.

The Integrated Terrestrial Ecosystem Carbon (InTEC) model was used to simulate disturbance and non-disturbance effects on the forest carbon cycle using these datasets (Chen et al., 2000). InTEC is a

combination of (i) Farqhuar's leaf-level photosynthesis model (Farqhuar et al., 1980) applied to remote sensing pixels through a spatial and temporal scaling scheme (Chen et al., 1999), (ii) CENTURY soil biogeochemical model (Parton et al., 1993) modified for forest applications (Chen et al., 2000); and (iii) an empirical forest regrowth model depending on air temperature (Chen et al., 2003b). Using InTEC with inputs from remote sensing and other spatial datasets, the carbon budget of Canada's forests was calculated at 1 km resolution in annual time steps. Figure 12 shows the carbon source and sink distribution in Canada's forests averaged over the last 15 years of the simulation (1984-1998). Compared with the forest age map (Figure 12), it is obvious that NBP is closely related to forest age. In BC, where most forests are older than 100 years, forests are near carbon neutral conditions because the small positive effects of warming (improved nutrient cycles) and CO_2 fertilization might have just offset the small decline in growth in aging forests. In prairie provinces, the overall forests are carbon sources due to frequent disturbances, and the increase in regrowth could not compensate for the dramatic increase in disturbance in 1980's and 1990's. Eastern and maritime provinces are generally carbon sinks because of large areas of productive forests gaining benefits from increased nitrogen deposition and improved nutrient conditions under warming conditions as well as a small effect of CO_2 fertilization. There is also a general gradient of decreasing sink strength from south to north because of the differential effects of warming on vegetation and soils. The decomposition of soil organic matter at higher latitudes is more sensitive to warming, while forest growth benefits less from warming at higher latitudes where vegetation is sparse. Critical to modeling these spatial patterns are remotely sensed forest fire patches and forest density (LAI). Partial validations of the results of soil and vegetation carbon stocks and carbon budgets were initially made against soil carbon data in Soil Landscape of Canada, aboveground biomass data in forest inventory, and four flux tower sites (Chen et al., 2003b) and were made further by Ju and Chen (1995) and Ju et al. (2006).

InTEC has also been used for estimating the carbon source and sink distribution in China's forests (Wang et al., 2007). The distribution is closely related to forest age distribution pattern. The results can be further improved with more detailed forest age information and more reliable NPP-age relationships for China's ecosystems. The current forest age structure in China has profound influence in the forest carbon budget in the next 100 years (Ju et al., 2007).

12. Summary

Satellite remote sensing provides an indispensible source of information to improve our estimates of the highly variable terrestrial carbon cycle in space and time. With our current computation capacity using common

personal computers, we can now easily afford spatially explicit, process-based carbon cycle modeling for large areas. For this purpose, the following main points are made through reviewing existing research results:

1. The spatial distribution of the gross primary productivity (GPP) can be reliably mapped using satellite data in recent years (in combination with meteorological and soil data). For accurate mapping of GPP, sunlit and shaded leaves must be separated and modeled individually. Big-leaf models (or its simpler form: light use efficiency models) are inaccurate and should be abandoned because these models don't adequately include the contributions of shaded leaves which can amount up to 50% of the total canopy photosynthesis.

2. The full forest carbon cycle involving biomass accumulation in the tree life cycle and soil carbon accumulation and decomposition has a long carbon residence time (15-50 years), and accurate modeling for all carbon cycle components requires a modeling length at least twice the carbon residence time. The spatial distribution of GPP obtained in recent years can be effectively combined with historical climate and atmospheric data for long-term carbon cycle modeling. GPP in a recent reference year can provide a reliable anchor point for such historical carbon cycle simulation.

3. Forest growth rates differ greatly in different stand development stages. Forest stand age is therefore a critical parameter for forest carbon cycle modeling. It not only provides information for the timing of the direct carbon emission during the last disturbance but also resets the clock for a new forest life cycle (regrowth, peak growth, and slow decline in growth). As demonstrated in the case study of Canada's forests, the regional carbon source and sink distribution is closely associated with the spatial distribution of forest stand age.

References

1. Abuelgasim, A. A., R. A. Fernandes, et al. (2006). "Evaluation of national and global LAI products derived from optical remote sensing instruments over Canada." IEEE Transactions on Geoscience and Remote Sensing 42: 1872-1884.
2. Amiro, B. D., J. B. Todd, et al. (2001). "Direct carbon emissions from Canadian forest fires,1959-1999." Can. J. For. Res. 31: 512-525.
3. Amthor, J. S. (1989). Respiration and crop productivity. New York.
4. Baldocchi, D. (1994). "An Analytical Solution for Coupled Leaf Photosynthesis and Stomatal Conductance Models." Tree Physiology(14): 1069-1079.
5. Baldocchi, D. (2001). "Fluxnet: a new tool to study the temporal and spatial variability of ecosystem-scale carbon dioxide, water vapour , and energy flux densities." Bulletin of the American Meteorological Society 82,: 2415-2434.
6. Ball, J. T. (1988). An analysis of stomatal conductance, Stanford University. **Ph. D.:** 89.
7. Baret, F., J. Morissette, et al. (2006). "Evaluation of the representativeness of networks of sites for the valiation of inter-comparison of global land biophysical products, Proposition of the CEOS-BELMANIP." IEEE Transactions on Geiscience and Remote Sensing 44(7): 1794-803.
8. Batjes, N.H., and J.A. Dijkshoorn. (1999). "Carbon and nitrogen stocks in the soils of the Amazon region." Geoderma

89:273–286.

9. Black, T. A., G. d. Hartog, et al. (1996). "Annual cycle of water vapour and carbon dioxide fluxes in and above a boreal aspen forest." Global Change Biology 2: 101-111.
10. Bonan, G. B. (1995). " Land-atmosphere CO2 exchange simulated by a land surface process model coupled to an atmospheric general circulation model." Journal of Geophysical Research 100: 2817-2831.
11. Canadell, J., C. L. Quéré, et al. (2007). Contributions to accelerating atmospheric CO2 growth from economic activity, carbon intensity, and efficiency of natural sinks. Proceedings of National Academy of Sciences.
12. Chen, J. M. (1996). "Canopy architecture and remote sensing of the fraction of photosynthetically active radiation in boreal conifer stands." IEEE Transactions on Geoscience and Remote Sensing 34: 1353-1368.
13. Chen, J. M. (1996). "Optically-based methods for measuring seasonal variation in leaf area index of boreal conifer forests." Agricultural and Forest Meteorology 80: 135-163.
14. Chen, J. M. (2005). "Satellite Imagery for Mapping the Carbon Source and Sink Distribution in Canada's Forests and Wetlands." Physics in Canada 61: 7-14.
15. Chen, J. M. and T. A. Black (1992). "Defining leaf area index for non-flat leaves." Plant, Cell and Environment 15: 421-429.
16. Chen, J. M., X. Chen, et al. (2005). "Distributed hydrological model for mapping evapotranspiration in a forested watershed." Journal of Hydrology 305: 15-39.
17. Chen, J. M., W. Chen, J. Liu, J. Cihlar, 2000. "Annual carbon balance of Canada's forests during 1895-1996." *Global Biogeochemical Cycle*14: 839-850.
18. Chen, J. M. and J. Cihlar (1995). "Plant canopy gap size analysis theory for improving optical measurements of leaf area index." Applied Optics 34: 6211-6222.
19. Chen, J. M. and J. Cihlar (1997). "A hotspot function in a simple bidirectional reflectance model for satellite applications." Journal of Geophysical Research 102: 25,907-25,913.
20. Chen, J. M., G. Mo, J. Pisek, F. Deng, M. Ishozawa, D. Chan. (2010). Foliage clumping index as an important structural parameter for estimating global terrestrial gross primary productivity. Global Biogeochemical Cycles (in review).
21. Chen, J. M., J. Liu, S. G., Leblanc, R. Lacaze, and J.-L. Roujean, (2003a). Multi-angular optical remote sensing for assessing vegetation structure and carbon absorption. *Remote Sensing of Environment,* 84: 516-525
22. Chen, J. M., W. Ju, et al. (2003b). "Spatial distribution of carbon sources and sinks in Canada's forests based on remote sensing." Tellus 55(2): 622-642.
23. Chen, J. M. and S. Leblanc (1997). "A 4-scale bidirectional reflection model based on canopy architecture." IEEE Transactions on Geoscience and Remote Sensing 35: 1316-1337.
24. Chen, J. M. and S. G. Leblanc, (2001). Multiple-scattering scheme useful for hyperspectral geometrical optical modelling. *IEEE Transactions on Geoscience and Remote Sensing,* 39(5): 1061-1071.
25. Chen, J. M., J. Liu, et al. (1999). "Daily canopy photosynthesis model through temporal and spatial scaling for remote sensing applications." Ecological Modelling 124: 99-119.
26. Chen, J. M., J. Liu, S. G., Leblanc, R. Lacaze, and J.-L. Roujean.(2003a). "Multi-angular optical remote sensing for assessing vegetation structure and carbon absorption." *Remote Sensing of Environment,* **84**: 516-525
27. Chen, J. M., J. Liu, et al. (2001). Utility of Multi-angle Remote Sensing for Terrestrial Carbon Cycle Modeling. Proceedings of the 8th International Symposium on Physical Signatures and Measurements in Remote Sensing. Aussois, France.
28. Chen, J. M., G. Pavlic, et al. (2002). "Validation of Canada-wide leaf area index maps using ground measurements and high and moderate resolution satellite imagery." Remote Sensing of Environment 80: 165-184.
29. Chen, J. M., P. M. Rich, et al. (1997). "Leaf area index of boreal forests: theory, techniques and measurements." Journal of Geophysical Research 102: 29,429-29,444.
30. Collatz, G. J., J. T. Ball, et al. (1991). "Physiological and environmental regulation of stomatal conductance, photosynthesis and transpiration: a model that includes a laminar boundary layer." Agricultural and Forest Meteorology 54(107-136).
31. Coursolle, C., H. A. Margolis, et al. (2006). "Late-summer carbon fluxes from Canadian forests and peatlands along an

east-west continental transect." *Canadian Journal of Forest Research,* 36: 783-800.

32. Cox, P. M., C. Huntingford, et al. (1998). "A canopy conductance and photosynthesis model for use in a GCM land surface scheme." J. Hydrol 212-213: 79-94.
33. Crisp, D. and C. Johnson. (2005). "The Orbiting Carbon Observatory Mission,." ACTA Astronautica 56(1-2): 193-197.
34. Dai, Y., X. Zeng, et al. (2003). "The Common Land Model (CLM)." Bull. of Amer. Meter. Soc. 84: 1013-1023.
35. Deng, F., J. M. Chen, et al. (2006). "Global LAI algorithm integrating the bidirectional information." IEEE Transactions on Geoscience and Remote Sensing 44: 2219-2229.
36. Deng, F., J. M. Chen, et al. (2007). "Global monthly CO2 flux inversion with focus over North America." Tellus 59B: 179-190.
37. Dickinson, R. E., M. Shaikh, et al. (1998). "Interactive canopies for a climate model." J. Clim 11: 2823-2836.
38. Farquhar, G. D. and S. v. Caemmerer (1982). Modelling of photosynthetic response to environmental conditions. Spring Verlag, Berlin, Germany.
39. Farquhar, G. D., S. v. Caemmerer, et al. (1980). "A biochemical model of photosynthetic CO2 assimilation in leaves of C3¬ species." Planta 149: 78-90.
40. Feng, X., G. Liu, et al. (2007). "Simulating net primary productivity of terrestrial ecosystems in China using a process model driven by remote sensing." Journal of Environmental Management 85: 563-573.
41. Fernandes, R. A., C. S. Butson, et al. (2003). "Landsat-5 and Landsat-7 ETM+ based accuracy assessment of leaf area index products for Canada derived from SPOT-4 VEGETATION data." Canadian Journal of Remote Sensing 29: 241-258.
42. Foley, J. A. (1994). "Net primary productivity in the terrestrial biosphere: The application of a global model." Journal of Geophysical Research 99: 20773-20783.
43. Foley, J. A., I. C. Prentice, et al. (1996). "An integrated biosphere model of land surface processes, terrestrial carbon balance and vegetation dynamics." Global Biogeochemical Cycles 10: 603-628.
44. Friedlingstein P., P. Cox,et al. (2006). Climate–Carbon Cycle Feedback Analysis: Results from the C4MIP Model Intercomparison, Journal Of Climate, 19, 3337-3353.
45. Garrigues, S., R. Lacaze, F. Baret, J. T. Morisette, M. Weiss, J. E. Nickeson, R. Fernandes, S. Plummer, N. V. Shabanov, R. B. Myneni, Y. Knyanzikhin, and W. Yang. 2008. Validation and intercomparison of global leaf area index products derived from remote sensing data. Journal of Geophysical Research, 113, G02028, doi:10.1029/2007JG000635.
46. Gholz, H. L., D. A. Wedin, et al. (2000). "Long-term Dynamics of pine and hardwood litter in contrasting environments: toward a global model of decomposition." Global Change Biology 6: 751-765.
47. Goetz, S. J., A. G. Bunn, et al. (2005). Satellite observed photosynthetic trends across boreal North America associated with climate and fire disturbance. Proceedings of the National Academy of Science. 38: 13521-13525.
48. Goulden, M. L., B. C. Daube, et al. (1997). "Physiological responses of a black spruce forest to weather." Journal of Geophysical Research 102: 28,987-28,996.
49. Goulden, M. L., J. W. Munger, et al. (1996). "Exchange of carbon dioxide by a deciduous forest: response to interannual climate variability." Science 271: 1576-1578.
50. Gurney, K. R., R. M. Law, et al. (2002). "Towards robust regional estimates of CO2 sources and sinks using atmospheric transport models." Nature 415: 626-630.
51. He, L., J. M. Chen, S. Zhang, G. Gomez, Y. Pan, K. McCullough, R. Birdsey, and J. Masek. 2010a "Normalized Algorithm for Mapping and Dating Forest Disturbances and Regrowth for the United States." *International Journal of Applied Earth Observation and Geoinformation* (in review).
52. He, L., J. M. Chen, R. Birdsey, and Y. Pan. 2010b. Relationships between net primary productivity and stand age derived using Forest Inventory and Analysis data and remote sensing imagery. *Global Change Biology* (in review).
53. Houghton, R. A. (2007). "Balancing the global carbon budget. Annual Review of Earth and Planetary." Sciences 35: 313-347.
54. Houghton, R. A. and J. L. Hackler (2003). "Sources and sinks of carbon from land-use change in China." Global Biogeochemical Cycles 17(2).

55. Hunt, E. R. J. and S. W. Running (1992). "Simulated dry matter yields for aspen and spruce stand in the North American Boreal Forest." Canadian Journal for Remote Sensing 18: 126-133.

56. Inoue, G. and G. Team (2006). "Global carbon dioxide and metane column observation by GOSAT (Greenhouse gases observing satellite)." Geophysical Research Abstracts 8: 10624-10625.

57. Jarvis, P. G. and J. I. L. Morison (1981). Stomatal control of transpiration and photosynthesis. In: "Stomatal Physiology". New York, Cambridge University Press.

58. Jonckneere, I., S. Fleck, et al. (2004). "eview of methods for insitue leaf area index determination. Part I: theries, sensors and hemisperhical photography." Agricultural and Forest Meteorology 121: 19-35.

59. Ju, W., J. M. Chen, et al. (2006). "Hydrological Effects on Carbon Cycles of Canada's Forests and Wetlands." Tellus B58: 16-30.

60. Ju, W., J. M. Chen, et al. (2007). "Future carbon balance of China's forests under climate change and increasing CO2." Journal of Environmental Management 85(3): 538-562

61. Kasischke, E. S., K. P. O'Neill, et al. (2000). Controls on patterns of biomass burning in Alaska boreal forests. Fire, Climate Change and Carbon Cycling in the Boreal Forest. E. S. Kasischke and B. J. Stocks. Springer-Verlag New York.

62.Kimball, J. S., P. E. Thornton, et al. (1997). "Simulating forest productivity and surface-atmosphere carbon exchange in the BOREAS study region." Tree Physiology 17: 589-599.

63. Krinner, G., N. Viovy, et al. (2005). "A dynamic global vegetation model for studies of the coupled atmosphere-biosphere system." *Global Biogeochemical Cycles,* 19,GB1015, doi:10.1029/2003GB002199.

64. Knorr, W. (2000). "Annual and interannual CO2 exchanges of the terrestrial biosphere: Process based simulations and uncertainties." Global Ecol. Biogeogr. 9: 225-252.

65. Kurz, W. A. and M. J. Apps (1999). "A 70-year retrospective analysis of carbon fluxes in the Canadian forest sector." Ecological Modelling 9(2): 526-547.

66. Lacaze, R., J. M. Chen, et al. (2002). "Retrieval of vegetation clumping index using hot spot signatures measured by POLDER instrument." Remote Sensing of Environment 79: 84-95.

67. Lacaze, R., P. Richaume, et al. (2003). Advanced algorithms of ADEOS2/POLDER-2 land surface process line : application to the ADEOS-1/POLDER-1 data. IGARSS 2003. Toulouse, France.

68. Lavigne, M. B. and M. G. Ryan (1997). "Growth and maintenance respiration rates of aspen, black spruce and jack pine stems at northern and southern BOREAS sites." Tree Physiology 17: 543-551.

69. Law, B. E., O. J. Sun, et al. (2003). "Changes in carbon storage and fluxes in a chronosequence of ponderosa pine." Global Change Biology 9: 510-524.

70. Le Quéré, C., M. R. Raupach, J. G. Canadell, G. Marland, et al. 2009. Trends in the sources and sinks of carbon dioxide. Nature Geoscience, DOI:10.1038/NGEO689.

71. Leblanc, S. G., J. M. Chen, et al. (2005). "Canada-wide foliage clumping index mapping from multi-angular POLDER measurements." Canadian Journal of Remote Sensing 31: 364-376.

72. Leuning, R. (1990). "Modelling Stomatal Behaviour and Photosynthesis of Eucalyptus grandis." Aust. J. Plant Physiol 17: 159-175.

73. Leuning, R., F. M. Kelliher, et al. (1995). "Leaf nitrogen, photosynthesis, conductance and transpiration: scaling from leaves to canopies." Plant Cell Environ. 18: 1183--1200.

74. Leuning, R., F. M. Kelliher, D. G. G. De Pury, and E.-D. Schulze. (1995). "Leaf nitrogen, photosynthesis, conductance and transpiration: scaling from leaves to canopies." Plant, Cell and Environment 18, 1183-1200.

75. Liu, J., J. M. Chen, et al. (2002). "Remote sensing based estimation of net primary productivity over Canadian landmass." Global Ecology and Biogeography 11: 115-129.

76. Liu, J., J. M. Chen, et al. (1997). "A process-based boreal ecosystem productivity simulator using remote sensing inputs." Remote Sensing of Environment 62: 158-175.

77. Liu, J. X., D. T. Price, et al. (2005). "Nitrogen Budget and Nitrogen controls on Ecosystem Carbon Sequestration: A Model

Implementation and Application to Saskatchewan, Canada." Ecological Modeling 186: 178-195.

78. Lloyd, J. and J. A. Taylor (1994). "On the temperature dependence of soil respiration." Functional Ecol. 8: 315-323.

79. Masek, J. G., E. F. Vermote, et al. (2006). "A Landsat surface reflectance dataset for North America, 1990-2000." Geoscience and Remote Sensing Letters, IEEE 3: 68-72.

80. Medlyn, B.E., F.-W. Badek, et al., (1999a). "Effects of elevated [CO2] on photosynthesis in European forest species: a meta-analysis of model parameters." Plant, Cell Environ. 22, 1475-1495.

81. Medlyn, B., M. Broadmeadow, (1999b). In Predicted Impacts of Rising Carbon Dioxide and Temperature on Forests in Europe at Stand Scale, Final Report ECOCRAFT ENVIRONMENT R&D ENV4-CT95-0077 IC20-CT96-0028, University of Edinburgh, UK.

82. Miller, E. E. and J. M. Norman (1971). "A sunfleck theory for plant canopies. I: lengths of sunlit segments along a transet." Agronomy J. 63: 735-738.

83. Myneni, R. B., S. Hoffman, et al. (2002). " Global products of vegetation leaf area and fraction of absorbed PAR from year one of MODIS data." Remote Sensing of Environment 83: 214-231.

84. Neeff, T. L. V. Dutra, J. R. dos Santos, C. C. Freitas, and L. S. Aruajo. (2005). "Tropical forest measurement by interferometric height modeling and P-Band radar backscatter." Forest Science, 51: 585-594.

85. Nilson, T. (1971). "A theoretical analysis of the frequency of gaps in plant stands." Agricultural and Forest Meteorology 8: 25-38.

86. Norman, J. M. (1982). Simulation of microclimates. Biometeorology in integrated pest management. J. L. Hatfield and I. J. Thomason. New York, Academic Press**:** 65-99.

87.Parton, W. J., D. S. Ojima, et al. (1993). "A general model for soil organic matter dynamics: sensitivity to litter chemistry, texture amd management." Soil Sci. Soc. Am. J.: 147-167.

88. Pataki, D. E., J. R. Ehleringer, et al. (2003). "The application and interpretation of Keeling plots in terrestrial carbon cycle research, Global Biogeochem." Cycles 17(1): 1022.

89. Peng, C. H., M. J. Apps, et al. (1998). "Simulating carbon dynamics along the Boreal Forest Transect Case Study (BFTCS) in central Canada 1. Model testing." Global Biogeochemical Cycle 12: 381-392.

90. Pisek, J., and J. M. Chen, 2007. "Comparison and validation of MODIS and VEGETATION global LAI products over four BigFoot sites in North America." *Remote Sensing of Environment,* 109: 81-94.

91. Pisek, J., J. M. Chen, and F. Deng, 2007. "Canada-wide validation of a new global leaf area index dataset from SPOT-4 VEGETATION data." *Canadian Journal of Remote Sensing,* 33: 1-16.

92. Pisek, J., J. M. Chen, R. Lacaze, O. Sonnentag, and K. Alikas. (2010). "Refining global mapping of foliage clumping index with multi-angular POLDER 3 measurements: topographic correction and preliminary validation." International Society of Photgrammetry and Remote Sensing (in press).

93. Potter, C. S., J. T. Ranserson, et al. (1993). "Terrestrail ecosystem production: a process model based on global satellite and surface data." Global Biogeochemical Cycles 7: 811-841.

94. Pury, D. G. G. D. and G. D. Farquhar (1997). "Simple scaling of photosynthesis from leaves to canopies without the errors of big-leaf models." Plant, Cell and Environment 20: 537-557.

95. Rödenbeck, C., S. Houweling, et al. (2003). "CO2 flux history 1982-2001 inferred from atmospheric data using a global inversion of atmospheric transport." Atmos. Chem. Phys. 3: 1919-1964.

96. Raulier, F., P. Y. Bernier, et al. (1999). "Canopy photosynthesis of sugar maple (Acer saccharum): comparing big-leaf and multilayer extrapolations of leaf-level measurements." Tree Physiology 19: 407-420.

97. Ross, J. 1981. The radiation regime and architecture of plant stands. Dr W. Junk Publishers

98. Running, S. W. and J. C. Coughlan (1988). "A general model of forest ecosystem processes for regional applications I. Hydrological balance, canopy gas exchange and primary production processes." Ecological Modelling 42: 125-154.

99. Running, S. W., R. R. Nemani, et al. (1989). "Mapping regional forest evapotranspiration and photosynthesis by coupling satellite data with ecosystem simulation." Ecology 70: 1090-1101.

100. Ryan, M., M. B. Lavigne, et al. (1997). "Annual carbon cost of autotrophic respiration in boreal forest ecosystems in relation to species and climate." Journal of Geophysical Research 102: 28871-28883.

101. Ryan, M. G. (1991). "Effects of climate change on plant respiration." Ecol. Appl. 1: 157-167.

102. Ryan, M. G., R. M. Hubbard, et al. (1996). "Autotrophic respiration in Pinus radiata in relation to nutrient status." Tree Physiology 16: 333-343.

103. Sarmiento, J. L., M. Gloor, N. Gruber, C. Beaulieu, A. R. Jacobson, S. M. Fletcher, S. Pacala, and K. Rodgers. 2009. "Trends and reginal distriubtuions of land and ocean carbon sinks." Biogeosciences Discussion 6:10583-10624.

104. Schut, P., J. Shields, et al. (1994). Soil Landscapes of Canada - An Environmental Reporting Tool. Canadian Conference on GIS Proceedings. Ottawa, Canada**:** 953-965.

105. Sellers, P. J., J. A. Berry, et al. (1992). "Canopy reflectance, photosynthesis, and transpiration. III. A reanalysis using improved leaf models and a new canopy integration scheme." Remote Sensing of Environment 42: 187-216.

106. Sellers, P. J., D. A. Randall, et al. (1996). "A revised land surface parameterization (SiB2) for atmospheric GCMs. Part I: Model formulation." Journal of Climate 9: 676-705.

107. Shields, J. A., C. Tarnocai, et al. (1991). Soil landscapes of Canada, procedures manual and user's hand boo. Ottawa, Ontario., Agric. Can. Publ. 1868/E, Agric. Can.

108. Smith, J. M., L. S. Heath, and J. C. Jenkins. (2002). Forest Volume-to-biomass models and estimates of mass for live and standing dead trees of US forests. Gneral technical report NE-298, Forest Service, US Department of Agriculture.

109. Smith, S. J. and J. A. Edmonds (2006). "The economic implications of carbon cycle uncertainty." Tellus 58B: 586-590.

110. Stephens, B. B., K. R. Gurney, et al. (2007). "Weak northern and strong tropical land carbon uptake from vertical profiles of atmospheric CO2." Science 316: 1732-1735.

111. Stenberg, P., M. Rautiainen, T. Manninen, P. Voipio and H. Smolander, "Reduced simple ratio better than NDVI for estimating LAI in Finnish pine and spruce stands", *Silva Fennica* 38, (1):3-14, (2004).

112. Stocks, B. J. (1991). The extent and impact of forest fires in northern circumpolar countries. Cambridge, MA, MIT Press.

113. Tans, P. P., I. Y. Fung, et al. (1990). "Observation Constraints on the global atmospheric CO2 budget." Science 247: 1431-1438.

114. Tarnocai, C. (1996). The amount of organic carbon in various soil orders and ecological provinces in Canada. Boca Raton, CRC Press.

115. Thomas, S. C., G. Malczewski, et al. (2007). "Assessing the potential of native tree species for carbon sequestration forestry in northeast China." Journal of Environmental Management 85(3): 663-671

116. Thompson, M. V., J. T. Randerson, et al. (1996). "Change in net primary production and heterotrophic respiration: How much is necessary to sustain the terrestrial carbon sink?" Global Biogeochem. Cycle 10: 711-726.

117. Trofymow, J. A. (1998). The Canadian Intersite Decomposition Experiment (DCIDET): Project and site establishment report**:** 15.

118. VEMAP (1995). "Vegetation/Ecosystem Modeling and Analysis Project: Comparing biogeography and biogeochemistry models in a continental-scale study of terrestrial ecosystem responses to climate change and CO2 doubling." Global Biogeochemical Cycles 9: 407-437.

119. Walker, B. and W. Steffen (1997). "An overview of the implications of global change for natural and managed terrestrial ecosystems." Conservation Ecology 1(2): 2.

120. Wang, S., J. M. Chen, et al. (2007). "Carbon sinks and sources in China's forests during 1901-2001." Journal of Environmental Management 85: 524-537.

121. Wang, Y.-P. and R. Leuning (1998). "A two-leaf model for canopy conductance, photosynthesis and partitioning of available energy I: Model description and comparison with a multi-layered model." Agricultural and Forest Meteorology 91: 89-111.

122. Wong, S. C., I. R. Cowan, et al. (1979). "Stomatal conductance correlates with photosynthetic capacity." Nature 282: 424-426.

123. Woodward, F. I., T. M. Smith, et al. (1995). "A global land primary productivity and phytogeography model." Global Biogeochemical Cycle 9: 471-490.

124. Wullschleger, S. D. (1993). "Biochemical limitations to carbon assimilation in C3 plants - A retrospective analysis of the A/Ci curves from 109 species." Journal of Experimental Botany 44: 907-920.

125. Zhang, Q., G. Pavlic, et al. (2004). "Deriving Stand Age Distribution in Boreal Forest Using SPOT VEGETATION and NOAA AVHRR Imagery." Remote Sensing of Environment, 91: 405-418.

Table 1. *Commonly used parameter values for photosynthesis and respiration in boreal conifer forests.*

Symbol	Unit	Meaning	Value	References
Photosynthesis				
g_{max}	mm s^{-1}	Maximum CO_2conductance	1.6	Dang et al. (1997) Running and Coughlan (1988)
g_{min}	mm s^{-1}	Minimum CO_2conductance	0.0	Chen et al. (1999）
N_{leaf}	%	Leaf nitrogen	1.2	Kimball et al. (1997)
N_m	%	Maximum leaf nitrogen	1.5	Bonan (1995)
$V_{m,25}$	μmol m^{-2} s^{-1}	Maximum carboxylation rate at 25 ^oC	33	Bonan (1995) Dang et al. (1999)
$PPFD_{coef}$	μmol m^{-2} s^{-1}	Coefficient in Eq. 28a	0.01	Kimball et al. (1997)
T_{opt}	^oC	Optimum temp.	25	Kimball et al. (1997)
T_{range}	^oC	Maximum temp. range	40	Kimball et al. (1997)
VPD_{open}	kPa	Water vapour deficit for maximum stomatal opening	0.2	Dang et al. (1997)
VPD_{close}	kPa	Water vapour deficit at stomatal closure	2	Dang et al. (1997)
Respiration				
Q_{10}	-	Temperature sensitivity	2.3	Kimball et al. (1997)
$r_{m,leaf}$	d^{-1}	Leaf respiration coefficient	0.002 at 20 ^oC	Kimball et al. (1997)
$r_{m,stem}$	g $g^{-1}d^{-1}$	Stem respiration coefficient	0.001 at 20 ^oC	Kimball et al. (1997)
$r_{m,rootc}$	g $g^{-1}d^{-1}$	Coarse root respiration coefficient	0.001 at 20 ^oC	Kimball et al. (1997)

$r_{m,rootf}$	g g^{-1}d	Fine root respiration coefficient	0.002 at 20 ^{o}C	Kimball et al. (1997)
r_g	g $g^{-1}d^{-1}$	Growth respiration coefficient	0.25	Ryan (1991)
$r_{g,root}$	g g^{-1}d	Root growth respiration coefficient	0.25	Ryan (1991)
$r_{a,root}$	-	Root carbon allocation coefficient	0.40	Running and Coughlan (1988)

(a) (b)

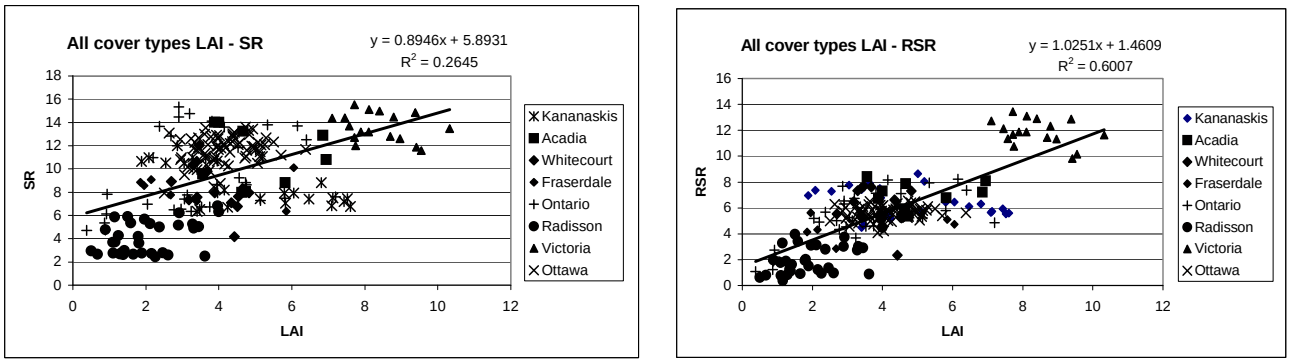

Figure 1. *Relationships between the leaf area index (LAI) and the simple ratio (SR) and between LAI and the reduced simple ratio (RSR) for all cover types in various locations in Canada, with deciduous forests and crops in Ottawa, deciduous forests in Ontario (several locations), and conifer forests in other locations (Chen et al., 2002).*

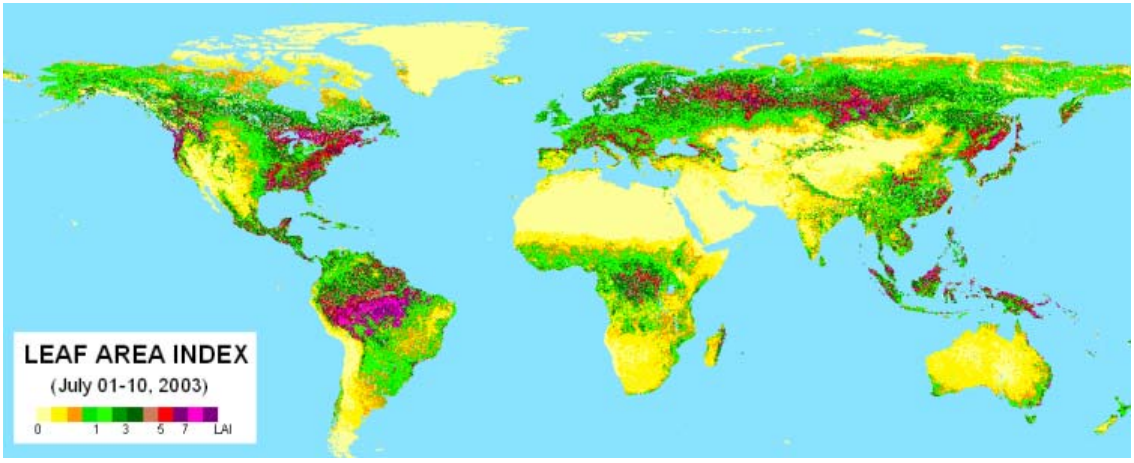

Figure 2. *An example of a global leaf area index map in July 1-10 in 2003 derived from VEGETATION data at 1 km resolution using the algorithm of Deng et al. (2006).*

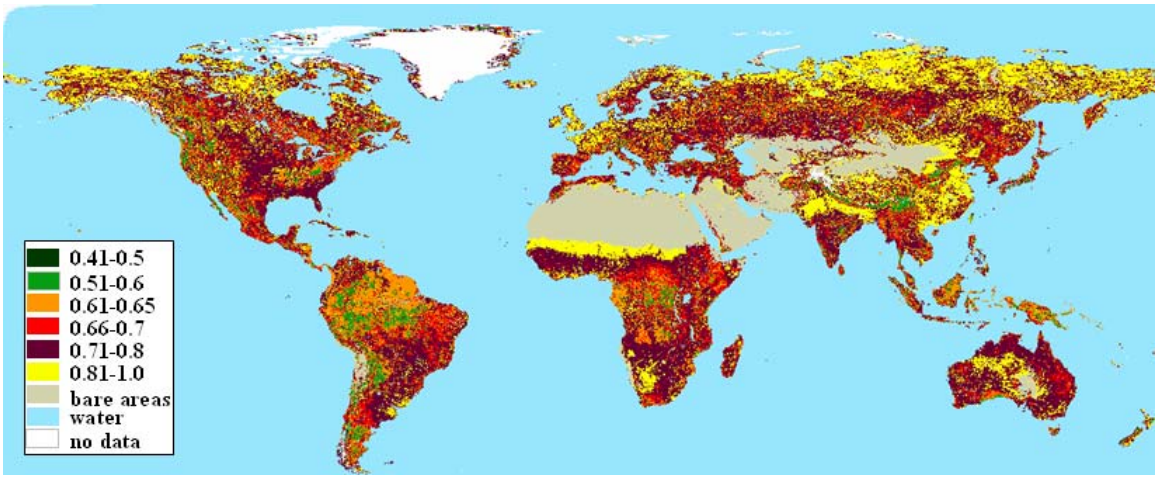

Figure 3. *Global clumping index map derived from POLDER III at 6 km resolution using the normalized difference between hotspot and darkspot (NDHD), updated based on Chen et al. (2005)*

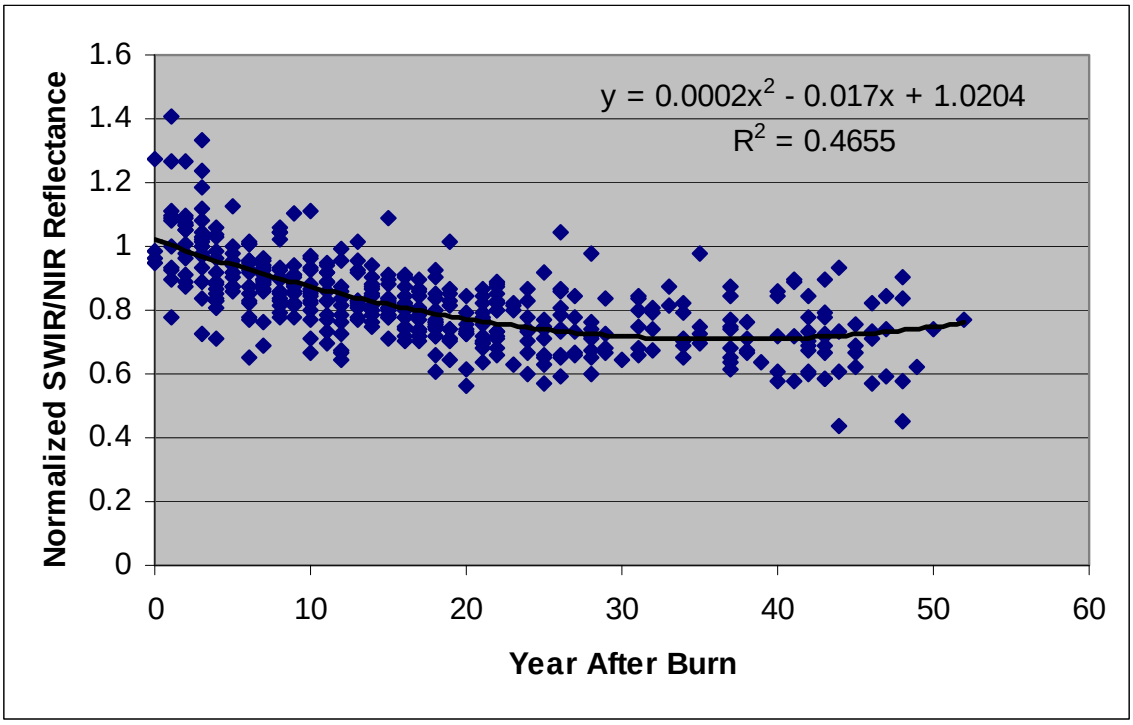

Figure 4. *The variation of the ratio between shortwave infrared (SWIR) and near infrared (NIR) reflectance with the time after burn. Note that the large initial decrease in the ratio and the asymptote at about 25 years after burn. Better correlations were found by separating them into 18 ecoregions in Canada (Amiro and Chen, 2002).*

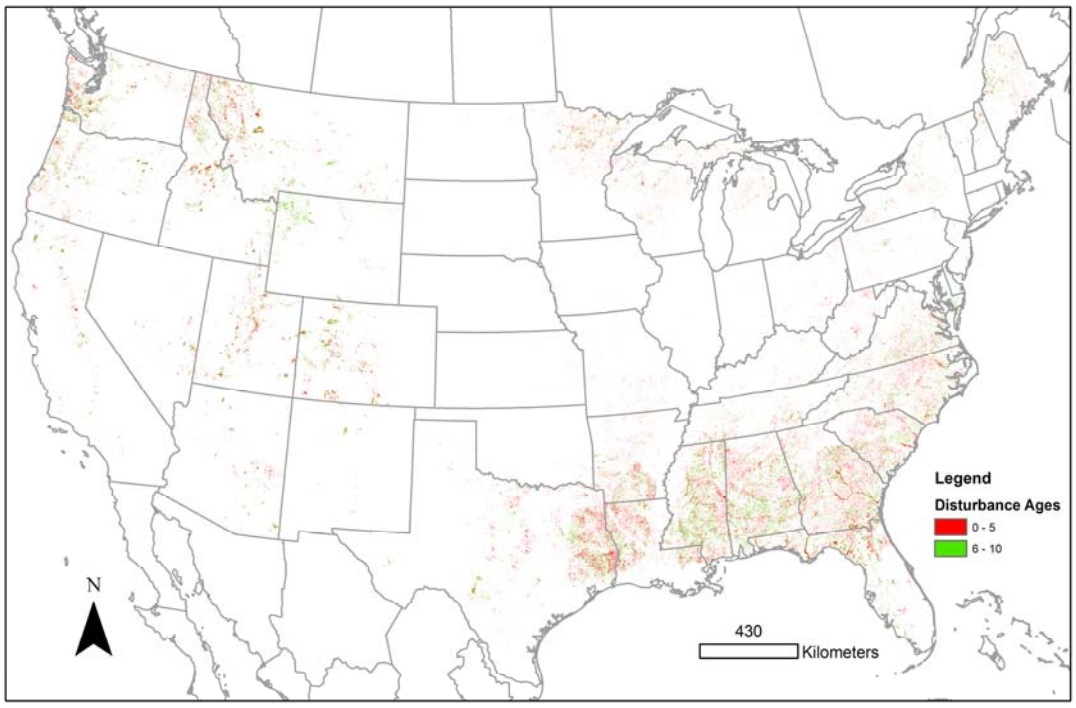

Figure 5. *Disturbed areas in the periods of 1990-1994 (green) and 1995-2000 (red) detected using Landsat images acquired circa 1990 and 2000 (He et al., 2010a). The images were preprocessed to 500 m resolution (Masek et al., 2008).*

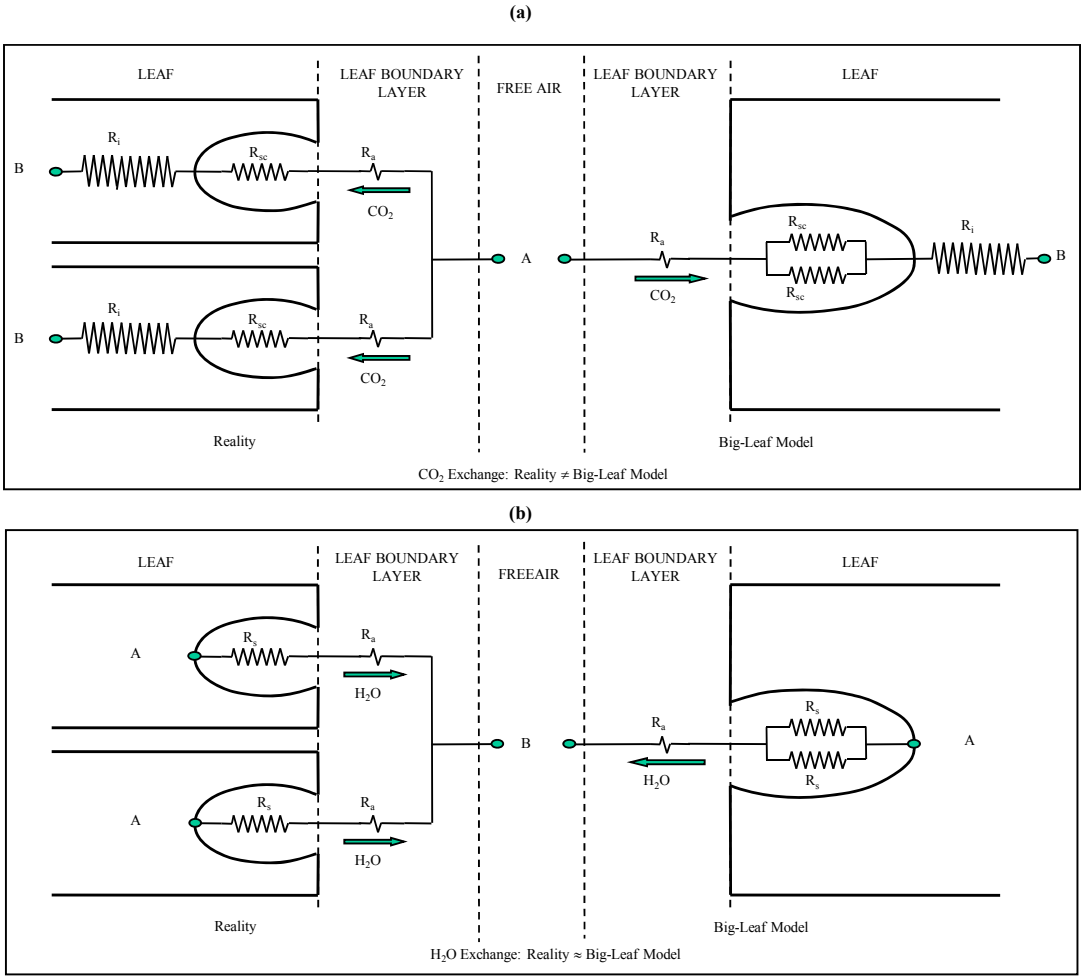

Figure 6. *Schematic of CO_2 and H_2O flow paths in a plant canopy. Panel (a) is for the CO_2 flow, and Panel (b) is for the H_2O flow. In both panels, the right hand side shows a big-leaf model and the left hand side represents the reality. Here, we only use two layers of leaves to represent the canopy. R_{sc} and R_s represent stomatal resistances to CO_2 and H_2O, respectively. R_i and R_a denote the leaf internal resistance and leaf boundary layer resistance, respectively. From the ways these resistances are combined, we can infer that the big-leaf model does not represent reality of the CO_2 flow (from A to B), but it can approximate well the reality of the H_2O flow (from A to B). Note that: (1) the influence of R_a is normally very small, and (2) R_i is very large and only exists for CO_2.*

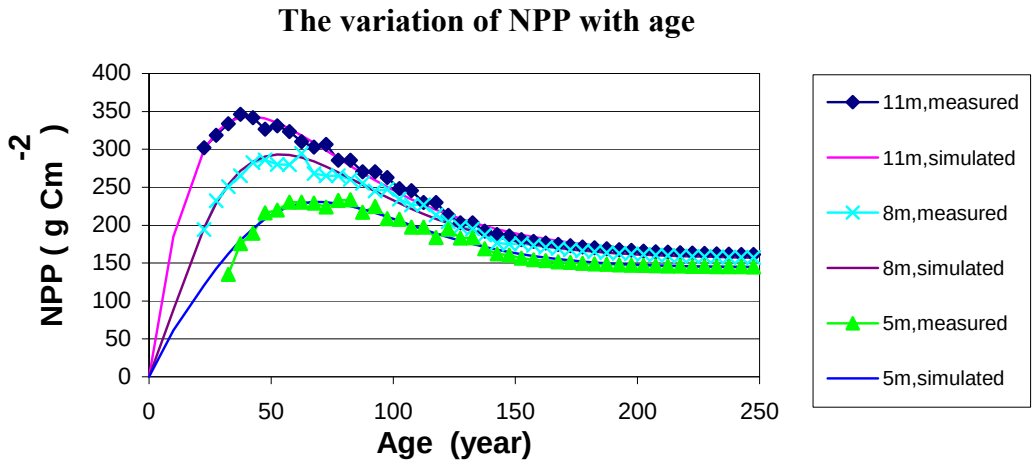

Figure 7. *The variation of net primary productivity (NPP) with forest stand age under different site indices (tree height in m in 50 years). The data used to derive these relationships are from black spruce stands in Ontario, Canada (Chen et al., 2002).*

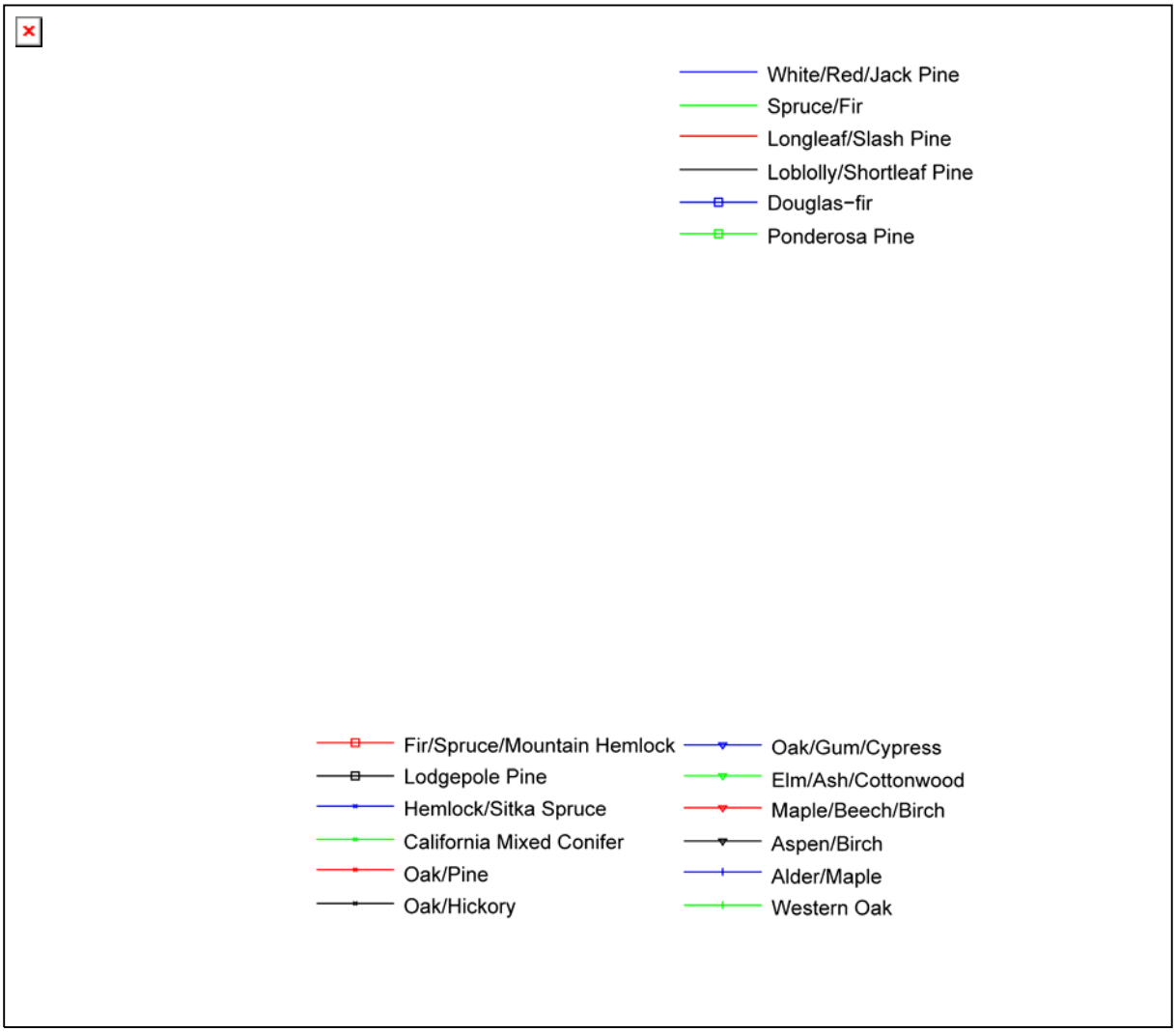

Figure 8, *NPP-age relationships for 18 forest species groups in USA, derived from Forest Inventory and Analysis data, a remotely sensed LAI image and a forest age map.*

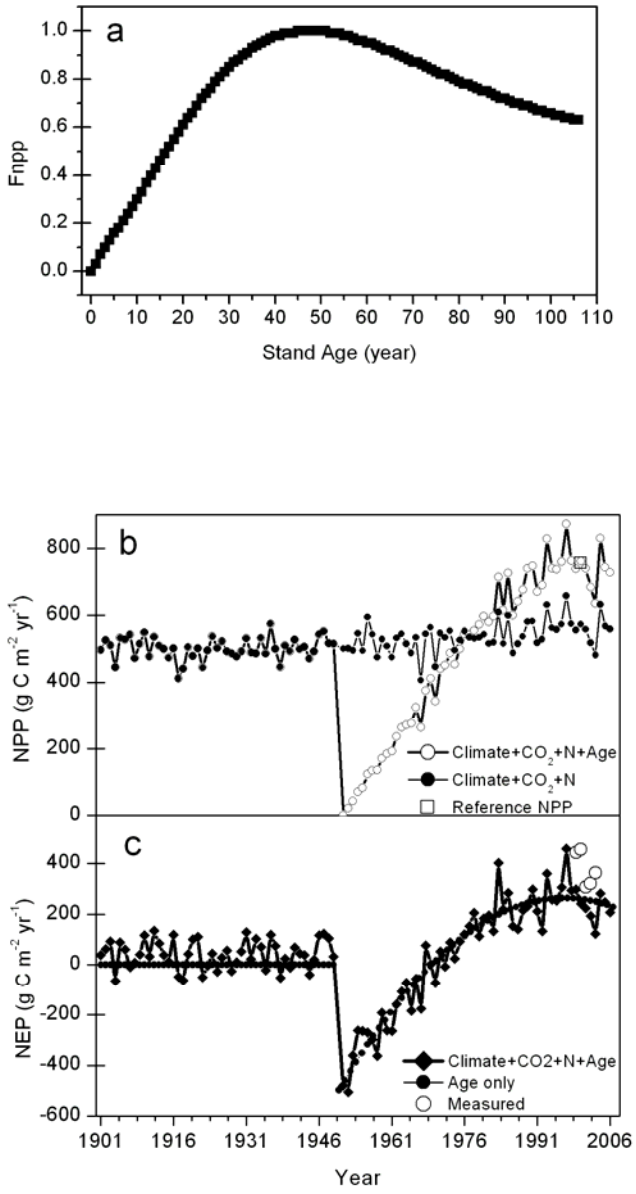

Figure 9*, An example of modeling the historical NPP and NEP for a conifer forest site in North America with consideration of the influences of climate (temperature, precipitation) and atmospheric (CO_2 concentration and nitrogen deposition) changes as well as disturbance and regrowth. (a) a normalized NPP-age curve for the forest species, (b) separating the effect of forest stand age on NPP from other factors, and (c) modeled historical variation in NEP in comparison with eddy-covariance measurements made at this site in recent years.*

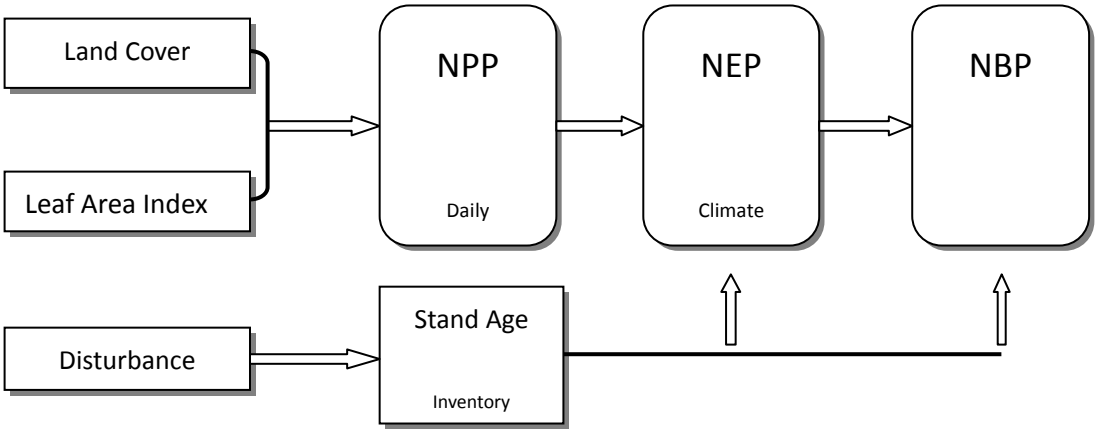

Figure 10. *Several major steps in using remote sensing data for terrestrial carbon cycle simulations. Land cover, leaf area index and fire scar derived from remote sensing are important input parameters. These parameters contribute differently to the estimation of net primary productivity (NPP), net ecosystem productivity (NEP) and net biome productivity (NBP). NBP represents the carbon source or sink.*

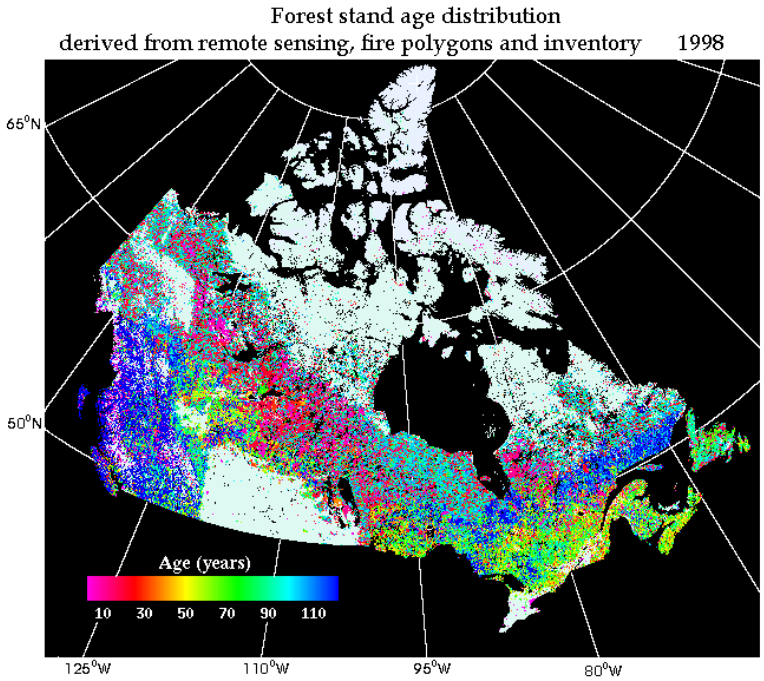

Figure 11. *Forest stand age distribution in Canada. This map integrates forest inventory data in the last 90 years (forest age is separated into 6 classes), large fire polygons since 1959, fire scar in the last 25 years detected using satellite remote sensing data. Forest regrowth is assumed to start in the second year after disturbance.*

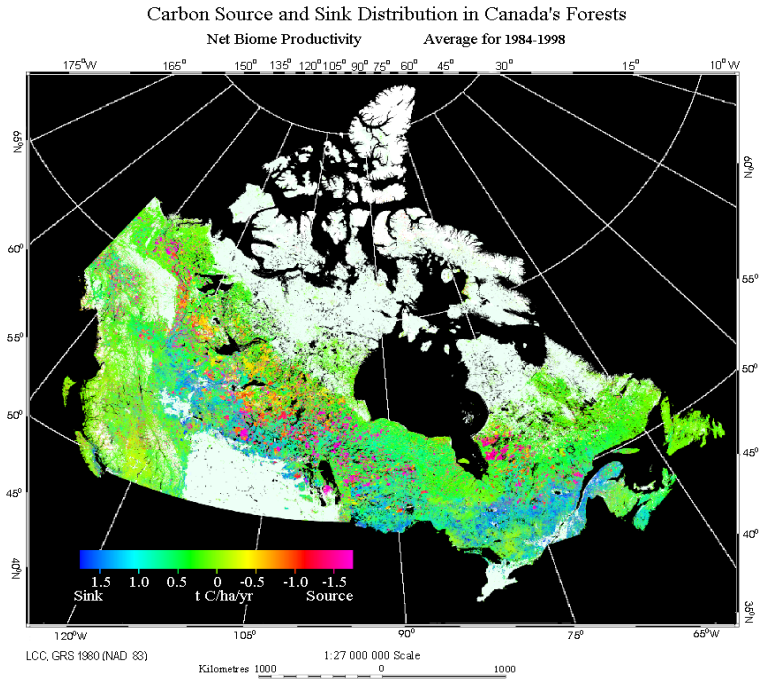

Figure 12. *Carbon source and sink (NBP) distribution in Canada's forest in 1984-1998. NBP includes the net primary productivity (NPP) minus heterotrophic respiration and the direct carbon emission due to disturbance. Due to data limitation, all disturbance (including fire, insect and harvest) is treated as fire disturbance in this example.*

（1 March 2010;accepted 30 May 2010）